J. Fluid Mech. (1984), *vol.* 141, *pp.* 391–429
Printed in Great Britain

The application of laser-induced Rayleigh light scattering to the study of turbulent mixing

By WILLIAM M. PITTS AND TAKASHI KASHIWAGI
Center for Fire Research, National Bureau of Standards, Washington, D.C. 20234

(Received 1 March 1983)

This work describes the development and characterization of an experimental system employing laser-induced Rayleigh light scattering with digital data acquisition as a time-resolved quantitative concentration probe in the turbulent flow field of a binary gas mixture. Equations for the expected signal and noise levels are given. Estimates of these parameters for the experimental system used here are in satisfactory agreement with experiment. It is demonstrated that the laser Rayleigh-light-scattering technique provides measurements having high spatial and temporal resolution for various locations within the concentration flow field. Measurements at various positions in the flow field of an axisymmetric methane jet issuing into a slow flow of air are reported and, where possible, compared with appropriate literature results. The statistical properties of the turbulent concentration fluctuations are found to be in good agreement with other independent measurements. Conditionally sampled measurements are also reported and shown to behave in the same manner as the limited number of similar measurements in the literature. The capability of calculating power spectra and correlation functions for the time behaviour of the methane concentration is also demonstrated. Raman and Rayleigh scattering techniques are compared as measurement techniques of scalar values in turbulent flow fields.

1. Introduction

Despite years of study, a full understanding of turbulent behaviour remains elusive. This is unfortunate, since turbulence occurs in many natural and man-made systems. Turbulent flow is the most effective means of mixing two or more fluids, and for this reason it is especially important in combustion and reaction systems, where mixing must precede molecular interactions. For this reason, understanding chemically reacting turbulent flows is a key to the more effective utilization of natural resources and the control of pollution. Development of effective turbulence models is essential for the design and construction of systems that utilize turbulent mixing most effectively. An understanding of this phenomenon is so critical that turbulence is often said to be the most important unsolved problem in physics.

We have initiated an experimental programme with the long-term goal of enhancing the fundamental understanding of chemically reacting turbulent flow. Our goal is to generate detailed data which can be used to describe empirically the behaviour of such flows and to provide input for mathematical models designed to predict their behaviour. An approach to the problem has been chosen in which the effects of changes in density and temperature on turbulent behaviour are first isolated and evaluated for a well-defined and widely studied flow configuration. Once the effects of changes in these parameters are understood, it will be possible to isolate

the effects of the nonlinear coupling which occurs between a turbulent flow and a chemically reacting system.

The need for an accurate, time-resolved probe of concentration in the turbulent flow field led us to evaluate several experimental techniques for their effectiveness for such measurements. These included intrusive probes, such as those using hot wires, and more-modern non-intrusive optical techniques such as marker nephelometry, Raman scattering, and Rayleigh scattering. Based on our analysis, we have chosen laser-induced Rayleigh light scattering as the technique most suited to our particular measurement requirements. This decision is based on the relative sensitivity of the technique and its ability to perform non-intrusive measurements with high temporal and spatial resolution,

There have been two past studies reported in the literature which indicated that Rayleigh light scattering might be a suitable probe of concentration behaviour in turbulent flow systems (Graham, Grant & Jones 1974; Dyer 1979). This report describes the development of such a system and how it is used to perform scalar measurements and includes a detailed analysis of the spatial and temporal resolution which can be achieved. A wide variety of properties of the behaviour of concentration fluctuations for an axisymmetric turbulent jet of methane issuing into air are reported and compared with similar measurements available in the literature. We conclude that, for certain types of flows, Rayleigh scattering is an extremely powerful technique for turbulent flow field scalar measurements. An expanded version of this work is available (Pitts & Kashiwagi 1983).

2. Rayleigh scattering

2.1. *Description of Rayleigh scattering*

Rayleigh scattering refers to elastic (no shift in frequency) scattering of electromagnetic radiation which occurs when the electric field of the radiation interacts with the electric fields of atoms or molecules. In this case, we will be interested in visible light, but the equations are also valid for radiation in the infrared and ultraviolet. An excellent discussion of Rayleigh light scattering is given in the book by McCartney (1976).

For the purpose of this work we have assumed that the effects of rotational Raman scattering are negligible since the cross-section for this process is ~ 100 times smaller than that for Rayleigh scattering. It should be noted that it may be necessary to include Raman effects in order to predict observed depolarization ratios accurately.

The following discussion considers the special case of a vertically polarized laser beam passing through a gas. A suitable detector of scattered light is located perpendicular to the propagation direction of the laser and the electric field direction of the light. The collection optics of the detector are stopped down in such a manner that it observes only a small volume of space containing the laser beam. This hypothetical arrangement is very similar to that actually used in most experiments, including the one reported here. We now give equations describing the intensity and polarization behaviour of scattered radiation reaching the detector.

The intensity of Rayleigh scattering is often described by defining an angular cross-section σ for each individual molecule as the scattered power per unit solid angle (intensity) divided by the incident power per unit area (irradiance). For a gas of number density N consisting of isotropic molecules (all of the elements of the diagonalized polarizability tensor are equal) the angular cross-section is related to the index of refraction by

$$\sigma^{\mathrm{i}}(90^{\mathrm{c}}) = \frac{4\pi^2(n-1)^2}{N^2\lambda^4}, \tag{1}$$

where the superscript i refers to an isotropic molecule, n is the index of refraction of the gas and λ is the wavelength of the light. This expression is derived for an ideal gas, assuming $n-1 \ll 1$.

The intensity of Rayleigh scattering from a unit volume of pure gas at a constant temperature is directly proportional to the number density of the gas and the irradiance of the incident light source. The polarization of the scattered radiation can be characterized by defining $I_{\parallel}$ as the intensity of scattered light polarized parallel to the electric field of the incident light and $I_{\perp}$ as the intensity polarized perpendicular. For an isotropic molecule these relationships give

$$I_{\parallel}^{\mathrm{i}}(90°) = \sigma^{\mathrm{i}}(90°)\, N I_0, \tag{2}$$

$$I_{\perp}^{\mathrm{i}}(90°) = 0, \tag{3}$$

where I_0 is the incident laser light irradiance and N is the number density of the gas.

For anisotropic molecules at least two of the diagonalized elements of the polarizability tensor are not equal, and an incident radiation field will induce a dipole moment within the molecule which is, in general, not parallel to the electric field of the radiation. In this case $I_{\perp} \neq 0$. The effects of molecular anisotropy are usually treated by defining the depolarization ratio

$$\rho = I_{\perp}/I_{\parallel} \tag{4}$$

and using scattering theory to show that (1) must be modified so that the anisotropic angular scattering cross-section for linearly polarized light becomes

$$\sigma^{\mathrm{a}}(90°) = \frac{4\pi(n-1)^2}{N^2\lambda^4}\frac{3}{3-4\rho}. \tag{5}$$

Using (5) it can be shown that

$$I_{\parallel}^{\mathrm{a}}(90°) = \sigma^{\mathrm{a}}(90°)\, N I_0 \tag{6}$$

and

$$I_{\perp}^{\mathrm{a}}(90°) = \sigma^{\mathrm{a}}(90°)\, N\rho\, I_0. \tag{7}$$

Values of ρ for most molecules are small, but vary over a range from zero to as large as approximately 0.15.

Since the intensity of light scattered from individual molecules is additive, the total intensity of Rayleigh scattering from a mixture composed of M different gases can be written as

$$I_{\parallel}^{\mathrm{a}}(90°) = N\left(\sum_{j=1}^{M} \sigma_j^{\mathrm{a}}(90°)\, X_j\right) I_0, \tag{8}$$

$$I_{\perp}^{\mathrm{a}}(90°) = N\left(\sum_{j=1}^{M} \sigma_j^{\mathrm{a}}(90°)\, \rho_j\, X_j\right) I_0, \tag{9}$$

where X_j is the mole fraction of gas j, and the total number density of the mixture is $N = \Sigma_{j=1}^{M} N_j$. By using (8) and (9) along with the condition $\Sigma_{j=1}^{M} X_j = 1$, the mole fraction of each component in an isothermal mixture of three gases can be determined by measurements of $I_{\parallel}^{\mathrm{a}}(90°)$ and $I_{\perp}^{\mathrm{a}}(90°)$ providing each gas has different values of σ_j and ρ_j. However, if there are more than three gases in the mixture or if the values of σ_j and ρ_j are not different for each gas, the system will be underdetermined and it will be impossible to solve for individual X_j.

When the system is not isothermal the total number density of a constant-pressure

gas mixture is inversely proportional to temperature. In this case (8) and (9) can be rewritten as

$$I_{\parallel}^{a}(90°) = \frac{N_0 P}{RT}\left(\sum_{j=1}^{M} \sigma_j^{a}(90°)\, X_j\right) I_0, \tag{10}$$

$$I_{\perp}^{a}(90°) = \frac{N_0 P}{RT}\left(\sum_{j=1}^{M} \sigma_j^{a}(90°)\, \rho_j\, X_j\right) I_0, \tag{11}$$

where N_0 = Avogadro's number = 6.023×10^{23}, P is the total pressure, R is the gas constant and T is the temperature. Providing the values of σ_j and ρ_j are different for each gas and independent of temperature, the maximum number of properties which can be uniquely determined are the temperature and the mole fractions of two gases. It should be mentioned that the radiation scattered by gas molecules is spectrally broadened owing to molecular translational motion (Doppler broadening). An evaluation of the spectral broadening of Rayleigh scattered light can be used to derive a temperature in a turbulent flow measurement as shown by Robben (1975).

2.2. *Past uses of Rayleigh scattering as a probe in turbulent flow systems*

Several groups have used Rayleigh scattering as a probe of scalar fields in turbulent combustion. Since a combustion system contains more than two gases, the actual quantity measured depends on the conditions of the experiment and assumptions (expected to be very good) must be made to obtain meaningful results and overcome the non-specificity of this type of scattering. Measurements of total number density and temperature have been reported in premixed and diffusion flames for a variety of flow conditions (e.g. Pitz *et al.* 1976; Bill *et al.* 1981; Gouldin & Dandekar 1982; Müller-Dethlefs & Weinberg 1979; Dibble, Hollenbach & Rambach 1980; Dibble & Hollenbach 1981).

Rayleigh scattering has also been used for monitoring the concentration fluctuations which occur in isothermal turbulent flows (Graham *et al.* 1974; Dyer 1979). In these experiments, real-time concentration measurements were made for axisymmetric fuel jets issuing into a slow flow of surrounding air. As long as the scattering cross-sections of the two gases are not the same, a single measurement of total Rayleigh scattering intensity allows a determination of the mole fractions of the two components. In this case, (8) can be rewritten as

$$I(90°) = (\sigma_a X_a + \sigma_f X_f)\, N I_0, \tag{12}$$

where σ_a and σ_f are the observed 90° scattering cross-sections for air and fuel respectively. As long as the pressure and laser intensity remain constant, the only unknowns in the equation are X_a and X_f. The mass-conservation equation

$$X_a + X_f = 1 \tag{13}$$

provides the second relation necessary for the determination of X_a and X_f.

Graham *et al.* (1974) were the first to report Rayleigh scattering measurements of this type. These workers studied the fluctuations which occur in acoustically forced and unforced jets of methane into air. This work demonstrated that Rayleigh scattering can be used to observe concentration fluctuations in a turbulent flow system. Later, Dyer (1979) used the same technique to measure the average concentration and r.m.s. concentration fluctuations as a function of position in a jet of propane. This work also included results of autocorrelation measurements which allowed the integral timescale to be determined for known positions in the turbulent flow. Simple statistical arguments were provided indicating that measurements performed in this manner are very accurate.

2.3. *Expected signal and noise levels for Rayleigh-scattering measurements*

Equation (12) gives the intensity of light scattered in the perpendicular direction from a light source of known I_0. In order to relate this equation to the signal measured in an experiment, it is necessary to include the effects of the solid angle for the collection optics, optical losses, and detector efficiency. The following expressions have been derived in terms of photons (or events)/s. If the amplification characteristics of the photon detector are known, it is possible to convert photons/s to A/s for devices operated in the current mode.

The predicted photon detection rate during a laser Rayleigh scattering experiment when the laser is assumed to have a cylindrical profile within the observation volume of the collection optics is given by

$$R_P = I_L \eta_L l \Omega \eta_C \epsilon N \sum_{j=1}^{M} \sigma_j X_j, \tag{14}$$

where R_P = detected photoelectron rate (photons/s),
I_L = laser output (photons/s),
η_L = coefficient of optical transmission between the laser and observation volume,
l = length of observed volume element,
Ω = solid angle (steradians) of collection for scattered light,
η_C = coefficient of optical transmission between observation volume and detector,
ϵ = quantum yield of photomultiplier,
$N \sum_{j=1}^{M} \sigma_j X_j$ = Rayleigh scattering cross-section for gas of total number density N.

This equation is based on several assumptions, including (i) observations are made at right angles to the laser beam, (ii) polarization effects are absent, and (iii) Ω is small enough to avoid considering the angular dependence of Rayleigh scattering.

In order to obtain an estimate of the number of photons that should be detected in an actual experiment, R_P has been calculated assuming that scattering is induced from air by a 7 W argon-ion laser operating at 488 nm. Using parameters chosen to approximate those actually existing in our experimental system, the detection rate of photons is calculated to be $R_P = 8.3 \times 10^7$ photons/s.

The use of Rayleigh scattering as a concentration probe requires an estimate of the accuracy with which a measurement of a given scattering intensity can be made during a time period Δt. The detection of photons obeys Poisson statistics, which require that a repeated measurement of the number N_P of detected photons from a constant-intensity light source during Δt will have a variance equal to the average number of photons detected during Δt. This requirement is expressed as

$$\text{var}\,(N_P) = \langle N_P \rangle, \tag{15}$$

where $\langle N_P \rangle = \lim_{L\to\infty} \Sigma_{j=1}^{L} (N_P)_j / L$. The relative uncertainty in a measurement of N_P is given by

$$\frac{(\text{var}\,(N_P))^{\frac{1}{2}}}{\langle N_P \rangle} = \langle N_P \rangle^{-\frac{1}{2}} = \langle R_P \Delta t \rangle^{-\frac{1}{2}}. \tag{16}$$

The uncertainty in optical measurements due to Poisson statistics is sometimes called electronic shot noise. Equation (16) shows that in order to reduce the relative uncertainty in the measurement of a Rayleigh scattering intensity it is necessary to

lengthen the counting period or to increase R_P by increasing the intensity of light reaching the detector.

An estimate of the relative uncertainty in the intensity measurement of Rayleigh scattering from air for our experimental conditions can be obtained by the use of (16). For a one second counting time the predicted relative uncertainty is only 0.00011. However, for a one microsecond counting time the relative uncertainty is 0.11. Clearly, the minimum time resolution which can be obtained with Rayleigh light scattering concentration measurements depends on the maximum relative uncertainty that is tolerable in the experimental measurement.

There are often other sources of noise in scattering measurements which can interfere with accurate determinations of Rayleigh scattering intensity, such as source fluctuations, dark current, and background interference. Becker, Hottel & Williams (1967*a*) and Shaughnessy & Morton (1977) have given detailed discussions of such sources of noise in regards to scattering from particles (Mie scattering). Similar considerations are expected to be important for scattering from molecules. For the experiments reported here, we conclude that electronic shot noise is by far the largest noise factor and that other noise sources can be disregarded.

In this work Rayleigh scattering is used to produce a time record of concentration fluctuations occurring in a turbulent flow of fuel (methane) into a slow flow of air. The light that is detected by the photomultiplier consists of scattering from the molecules within the flow and background radiation from light scattered by the apparatus and other sources. It is therefore necessary to deconvolute the scattering due to actual Rayleigh scattering from background light. We have used a calibration procedure in which scattering from air and methane is measured before the turbulent flow of methane into air is initiated. These intensities are recorded for a relatively long time to ensure that the errors in the measurements due to photon statistics are small. The intensity of scattering from the turbulent flow is then recorded in an identical manner. The mole fraction of methane is then obtained directly from the equation

$$X_{CH_4} = \frac{I_{tur} - I_{air}}{I_{CH_4} - I_{air}}, \tag{17}$$

where I_{tur}, I_{air} and I_{CH_4} refer to observed intensities from the turbulent flow, air and methane respectively. This equation can easily be obtained from (12). Note that each intensity contains contributions from background radiation, but that the background contribution drops out when the differences in (17) are taken. The value of each X_{CH_4} will have an error due to electronic shot noise in the measurement of I_{tur}. Fortunately, methods exist for compensating statistically for electronic shot noise when calculating many of the quantities of interest for the turbulent flow. These techniques are considered in §3.

3. Calculational methods for properties of the concentration flow field

Our work uses Rayleigh light scattering as a probe of the time-resolved concentration fluctuations occurring in a turbulent flow. The raw data that are generated are digitized and stored in the memory of a minicomputer. This subsection describes how the data are analysed in order to describe the properties of the concentration fluctuations at a point in space.

The first requirement is to characterize the statistical distribution of the concentration fluctuations. We have chosen to do this by use of the average concentration and the second through fourth central moments of the distribution. We will report

the average $\overline{X}$, root-mean-square (r.m.s.) X', skewness S and kurtosis K. S and K can be considered as measures of how the experimental distribution differs from a Gaussian. For a perfect Gaussian $S = 0$ and $K = 3$.

In §2.3 it was pointed out that there is an electronic shot noise associated with every measurement of X_{CH_4} using (17). This noise can lead to large errors in the calculated values of X', S and K when it is comparable in size to the intensity changes in Rayleigh scattering due to concentration fluctuations. Fortunately, Birch *et al.* (1978) have developed a very effective mathematical method for separating the actual moments of the intensity fluctuations (due to concentration fluctuations) from the effects of shot noise. These workers used the earlier results of Pike (1969), who had shown that the moments of the photon-number distribution are identical with the factorial moments of the detected photon distribution.

In order to apply the results of Pike the detected Rayleigh scattering must be given as a series of numbers of detected photocounts, N_P, collected during the time period Δt. The factorial moments for the distribution of N_P are defined as

$$(\mu'_{(r)})_{PC} = \frac{\sum_{j=1}^{L} (N_P)_j^{(r)}}{L}, \tag{18}$$

where $\mu'_{(r)}$ is the rth factorial moment, the subscript PC indicates the photocount distribution, and

$$B^{(r)} = B(B-1)(B-2)\ldots(B-(r-1)) \quad \text{or} \quad B!/(B-r)!.$$

According to Pike (1969),

$$(\mu'_{(r)})_{PC} = (\mu'_r)_{PF}, \tag{19}$$

where $(\mu'_r)_{PF}$ are the moments of the photon-field distribution. $(\mu'_1)_{PF}$ is the average number of photocounts during Δt, and for scattering from a turbulent flow can be denoted $\bar{I}_{tur}$ and used in (17) to calculate $\overline{X}_{CH_4}$. In order to obtain the higher moments for the concentration distribution, the photon-field moments must be converted to central moments using the relation

$$(\mu_r)_{PF} = \sum_{j=1}^{r} (-1)^j \binom{r}{j} (\mu'_{r-j})_{PF} (\mu'_1)^j_{PF}, \tag{20}$$

and then normalized to include only the scattering from gases in the field of view of the photomultiplier:

$$\mu_r = \frac{(\mu_r)_{PF}}{(I_{CH_4} - I_{air})^r}, \tag{21}$$

where I_{CH_4} and I_{air} are the average numbers of photocounts defined earlier.

Power spectra $\Phi(\omega)$ are taken in order to determine the frequencies which compose the concentration fluctuations. The method known as the fast Fourier transform (FFT) due to Cooley & Tukey (1965) is used to quickly calculate the Fourier transform, and a simple complex multiplication then yields $\Phi(\omega)$. It should be noted that electronic shot noise is 'white'. This means that it is a constant intensity at all frequencies, and a power spectrum due to concentration fluctuations measured by Rayleigh scattering will be built on a flat base due to shot noise.

The correlation function $R(\tau)$ is also calculated for the concentration-data records. The minicomputer used in this study is programmed to calculate $R(\tau)$ by taking a FFT of $X(t)$, squaring the complex function that results, and taking the inverse Hermitian (reverse Fourier transform) of the square.

All of the functions describing the statistical behaviour of the time-dependent concentration fluctuations discussed thus far are averaged for the entire data set. However, it is well known that turbulent flows display a property known as intermittency (for a discussion see Schon & Charnay 1977), which is due to the presence of two distinct fluid behaviours in the instantaneous flow field. In this work we are interested in the intermittency function $I(t)$, which describes the passage of the turbulent/non-turbulent boundary of the fluid through the observation volume. We have defined a turbulent region as existing when air has been entrained into the flow and a non-turbulent region as one where either only air or methane are present. The following equations can be written to describe this concept mathematically:

$$\begin{aligned} I(t) &= 1 \quad (0 < X_{\mathrm{CH_4}}(t) < 1), \\ I(t) &= 0 \quad (X_{\mathrm{CH_4}}(t) = 0,\ X_{\mathrm{CH_4}}(t) = 1). \end{aligned} \tag{22}$$

This definition of turbulent intermittency based on concentration has been used by several research groups (Shaughnessy & Morton 1977; Becker, Hottel & Williams 1965, 1967*b*; Konrad 1976) and also in the similar case of heated flows where the marker is temperature (Antonia, Prabhu & Stephenson 1975). By simultaneously monitoring temperature and velocity, Chevray & Tutu (1978) demonstrated that the intermittency function derived by real-time monitoring of a temperature marker is nearly identical with that found when velocity fluctuations are used.

Even though intermittency is a very simple idea conceptually, in practice it has proven very difficult to generate a consensus among workers in the field on an experimental definition. In part this is due to the wide range of turbulence variables (e.g. velocity, vorticity, concentration) for which intermittency measurements have been made and the wide range of experimental techniques employed. In the case of velocity measurements the problem is severe, since there is fluid motion in non-turbulent regions and it is necessary to base intermittency decisions on whether or not the velocity fluctuations are characteristic of turbulent flow. For scalar quantities the problem is somewhat simplified, since the decision is usually based on the presence or absence of the scalar (e.g. heat or mass). For these measurements, the accuracy of the determination of the interface location is usually limited by noise in the measurement of the scalar quantity. An additional difficulty arises owing to the finite sampling volume of most probes. Fluctuations occurring in this volume are averaged and this can lead to inaccuracies in the determination of the boundary location. Many different approaches to solving or at least minimizing these problems have been used. In the experimental section (§4.5) we describe a procedure based purely on statistics and the noise level in the measurement.

Once an intermittency function is obtained, it can be used to calculate several new properties of the flow field. The fraction of time the observation volume spends within the turbulent flow region is defined by the intermittency factor γ. For discrete data an approximation of γ is calculated by summing the number of points at which $I(t) = 1$ and dividing by the total number of points. Clearly the accuracy of γ will depend on the size of the eddies being observed and the length of time for which the measurement is made. This point will be discussed further in later sections. An intermittency frequency, denoted by f_γ, can be defined as the average number of times $I(t)$ goes from 0 to 1 during a one second time period. It is obviously related to the number of large-scale structures passing through the observation volume. Unfortunately, values of f_γ have proved very difficult to reproduce among different laboratories. This observation is believed (Goldschmidt, Mulej & Ajagu 1979) to be due to the

presence of very short bursts of turbulence in the observation volume which do not significantly modify the value of γ, but which modify the value of f_γ dramatically depending on whether or not they are detected.

Values of $(\bar{X})_T$, $(X')_T$, $(S)_T$ and $(K)_T$ are obtained for the turbulent regions of the jet by conditionally sampling the concentration time profiles by multiplying by $I(t)$. Where electronic shot noise is important, (18)–(21) are used to deconvolute its effects.

4. Equipment and procedures

4.1. *Flow system*

The flow system used for this experiment consists of an axisymmetric jet of methane issuing into a slow flow of surrounding air. The jet is constructed from a 61 cm length of 6.35 mm inner diameter brass tubing (9.5 mm outer diameter). These dimensions ensure that fully developed pipe flow occurs in the tube before the methane exits. The output end of the tube is sharpened to a fine edge, and the upstream end is connected to a ballast chamber to minimize pressure fluctuations . Since Rayleigh-scattering measurements are extremely sensitive to interference from particle (Mie) scattering, it is necessary to enclose the entire flow system to prevent dust particles from reaching the observation volume. For this reason the jet is centred inside a $10.4 \times 10.4 \times 61$ cm^3 enclosure constructed from 5 mm thick optical crown glass. A flow of air enters the enclosure from the bottom after passing through a bed of polystyrene balls and a wire gauze to ensure a homogenous flow. Flows of both methane and air are controlled and measured by Fischer and Porter Flowrator meters.† Both flows are prefiltered with 0.3 micron filters to remove particles. Methane (Matheson Technical Grade, $> 98\,\%$) is obtained from a cylinder. A regulated, house airline is the source of air. All measurements reported here are for an initial methane flow velocity of 1020 cm/s and a surrounding air flow velocity of 34 cm/s. These velocities correspond to a Reynolds number of $Re = uD/\nu = 4130$, where u is the initial velocity of the methane flow, D is the diameter of the jet and ν is the kinematic viscosity of methane.

The jet and enclosure are mounted on a lathe bed to allow accurate positioning of the observation volume in the flow field. Scales mounted on the lathe bed give positions of the observation volume relative to the centre of the nozzle exit which are accurate to 0.25 mm.

4.2. *Optical system*

Figure 1 shows the optical system used in this study. A Spectra-Physics Model 171-19 Ar-ion laser is operated in the single-wavelength mode to produce a 7 W output at 488 nm. The laser beam is expanded to 22 mm using a $10\times$ beam expander from Special Optics and is then focused to a narrow cylinder of ~ 0.035 mm diameter within the system enclosure by a lens (focal length = 25 cm). The position of this focus along the laser beam is determined by a knife-edge test. The approximate length of the cylindrical region over which the focused laser-beam diameter remains constant is 4 mm.

Light scattered from the observation volume is collected and collimated by an anti-reflection (AR) coated 10.2 cm achromatic lens ($f/2$) and then refocused using

† Certain commercial equipment, instruments or materials are identified in this paper in order to adequately specify the experimental procedure. Such identification does not imply recommendation or endorsement by the National Bureau of Standards, nor does it imply that the materials or equipment are necessarily the best available for the purpose.

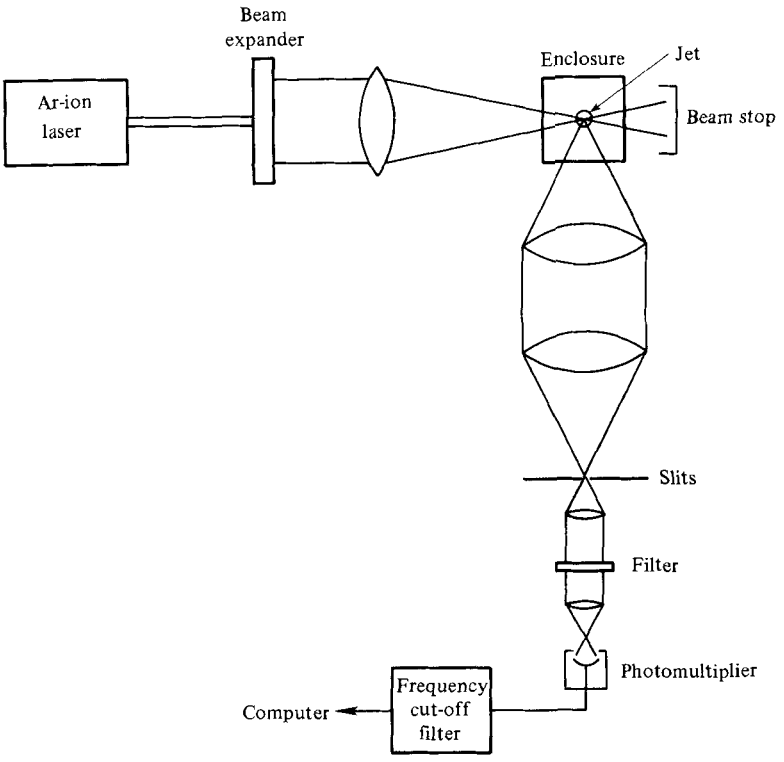

FIGURE 1. Optical arrangement and detection electronics for laser Rayleigh-light-scattering measurements.

a 10.2 cm AR coated spherical lens. A set of adjustable slits is placed at the focal point of the second lens to define the observation length of the cylindrical region of scattering. The diameter of the volume is determined by the diameter of the laser beam. By using the laser to back-illuminate a 0.025 mm pinhole, it is possible to determine the actual length of the observation volume by translating the pinhole along the laser-beam path. Spherical aberration limits the minimum optical resolution to be ~ 0.27 mm. The minimum volume element that can be resolved using the current optical system is estimated to be 0.0003 mm^3.

After passing through the slits, the light is again collimated with a 22.5 mm AR coated lens. It is then filtered by a Pomfret Research Optics narrow-bandpass filter centred at 488 nm and having a 1.2 nm FWHM and the maximum transmission of 60 %. Finally, a second 22.5 mm lens is used to focus the scattered light on the photocathode of a photomultiplier tube.

4.3. *Detection, conditioning and recording electronics*

The EMI 9781B photomultiplier tube used in this study has a modified S-5 photocathode with a reported quantum efficiency of 0.14. In all experiments described here the tube was operated at 680 V. The calibrated gain for this voltage is reported by the manufacturer as $G = 2.4 \times 10^6$.

The output of the photomultiplier is measured in the current mode. A variable resistor is used to convert the current into a voltage which is fed to an Ithaco Model 4302 dual filter employed as a low-pass 10 × amplifier. This filter provides a relatively sharp cut-off frequency which attenuates frequencies higher than a preset value at 24 dB/octave. Input voltages are adjusted so that a suitable output voltage (< 2 V)

is produced for signal acquisition. The time response of the electronics is such that the filter provides all frequency selection and smoothing of the photomultiplier signal. Generally a cut-off frequency of 5700 Hz was used.

After conditioning, the PM signal is fed to the 12 bit digitizer of a Nicolet 1180 data acquisition and processing system. Digitization rates were usually twice the cut-off frequency. The digitized input signal, which is proportional to the smoothed current output of the photomultiplier, is stored in memory. Data sets as large as 32768 measurements can be recorded in a single scan. At the conclusion of a data-collection cycle the entire data set is transferred to a hard disc for later analysis.

4.4. *Experimental procedures*

We have chosen to measure the methane mole fraction using (17). This equation requires that only relative Rayleigh scattering intensities and not absolute quantities be measured. For each turbulence measurement it is necessary to measure the scattering intensity due to methane and air. Data records of 4096 points are taken for each gas. Software programs are available for rapidly calculating average intensities and standard deviations. Statistical analysis indicates that the relative error due to photon statistics in these average-intensity measurements is much less than 1 %. An additional measurement is made when the enclosure is filled with helium. Since the cross-section for helium is only 0.015 of that for air, this intensity provides a good estimate of the background intensity from the enclosure in the absence of scattering gas. Owing to the small size of the enclosure and the use of glass walls with 4 % reflections at each air/glass interface, the amount of detected light that is not due to Rayleigh scattering is on the same order as the light scattered from air. This background light limits how close the observation volume can be placed to the nozzle, because scattering of the background light from the nozzle is quite strong. By subtracting the background intensity from the intensities observed when air and methane are in the enclosure, the intensity ratio $I_{CH_4}/I_{air} = \sigma_{CH_4}/\sigma_{air}$ can be calculated. This ratio is used as a check to ensure that no systematic errors are being made in the measurements. An indication of the reproducibility of the measurements can be found in the average value of $\sigma_{CH_4}/\sigma_{air} = 2.33 \pm 0.02$ found for ten different data sets recorded on the same day. Actual values of σ_{CH_4} and σ_{air} for ambient conditions are calculated using (1) and values of n_{air} and n_{CH_4} at 488 nm taken from tables in McCartney (1976) and Landolt-Börnstein (1962) respectively. The results are $\sigma_{air} = 8.17 \times 10^{-28}$ cm^2/sr and $\sigma_{CH_4} = 1.91 \times 10^{-27}$ cm^2/sr, giving a predicted value of 2.34 for $\sigma_{CH_4}/\sigma_{air}$. Agreement between observed and predicted values is excellent. As a final check of intensity calibrations, a second data set is recorded for air after the turbulence data have been taken. If the two intensities measured for air differ by more than 1 %, the entire series of measurements is repeated.

Immediately after calibrating the Rayleigh-scattering intensity, a turbulent flow of methane into air enters the enclosure. After allowing a sufficient period of time for the flow to flush the enclosure and to stabilize, the time behaviour of Rayleigh-scattering intensity is measured. The size of the turbulent data record can be varied, but for the experiments reported here either 16384 or 32768 real-time intensity measurements were recorded and stored on disc.

4.5. *Data analysis*

The properties of the concentration fluctuations discussed in §3 are calculated at different positions in the flow field. As previously noted, Rayleigh-scattering intensities recorded in the memory of the computer are only relative values and contain errors due to photon statistics. In order to apply (18)–(21) for the calculation of

concentration moments, it is necessary to know the actual numbers of photons detected. We have used (16) as a means of providing a calibration factor for changing the relative intensities into absolute numbers of detected photons. Measurements of scattering from air and methane provide relative light intensities for two well-defined methane concentrations. These measurements also yield the relative standard deviations. It is worthwhile to note that the ratio of the standard deviations for the two measurements is found, as expected, to be inversely proportional to the square root of the intensity ratio. By using the relative standard deviation for scattering from air and substituting in (16) it is possible to calculate an effective value for the number of photons detected during a period equal to the dwell time. This number provides the calibration factor necessary to scale all of the relative intensity measurements in the computer memory to numbers of detected photons. Software has been developed using (18)–(21) to calculate $\overline{X}$, X', S and K for the turbulent methane-concentration time histories.

Power spectra of concentration fluctuation data are calculated by first using routines provided by Nicolet to take the fast Fourier transform and then applying a complex multiplication to give the power spectrum. Power spectra of entire data sets give high-frequency resolution, but result in a large amount of digital noise. For this reason, the data are broken into smaller data records of 1024 data points. Fourier transforms for each of these smaller records are averaged and a power spectrum taken of the average. Even though the resulting power spectrum has much less frequency resolution, the digital noise is greatly reduced. This method of calculating power spectra from digital data has often been applied before (for examples see Konrad 1976; Cheng, Bill & Robben 1981).

Correlation functions for the turbulent concentration data records are calculated using a subroutine of Nicolet's general-applications package. The entire data record of 16384 or 32768 measurements is treated in a single calculation. Every data set recorded in this study gave $R(\tau)$ functions which could be fitted as exponentials. For this case, the Eulerian or integral timescale $\mathscr{T}$ can be written as

$$\mathscr{T} = \int_0^\infty R(\tau)\,\mathrm{d}\tau = \int_0^\infty \mathrm{e}^{-\tau/\mathscr{T}}\,\mathrm{d}\tau, \tag{23}$$

which is simply equal to the time constant for the decay of the correlation function. A linear least-squares fit is used to calculate $\mathscr{T}$ from the logarithm of the correlation function.

A simple algorithm has been developed for making intermittency decisions. These decisions are complicated by the relatively large error in the individual measurements due to Poisson noise. Clearly the ability to differentiate turbulent from non-turbulent fluid will depend on the noise level. As discussed above, this noise level is directly related to such factors as averaging time (cut-off frequency), laser power and observation volume. We have chosen to make intermittency decisions based purely on statistical grounds. The fluid is considered to have become turbulent when five 'independent' intensity measurements fall above the sum of the scattering intensity for air and one half of the standard deviation in the air measurement. The number of data points required to equal five independent measurements is calculated by dividing 5 by the product of the dwell time and the cut-off frequency. Using the above criterion, the probability that the gas contains a measurable concentration of methane is 0.997. The gas is defined as having returned to non-turbulent behaviour when the average of five independent measurements falls below the defined cut-off level. It should be noted that many other equally valid criteria could be selected to

define intermittency. Even though this prescription for calculating the intermittency function is somewhat arbitrary, it does yield results which are in agreement with visual inspections of the data and which behave very much like those reported in the literature. Additionally, it does seem to give results which are fairly independent of the cut-off frequency used for the experiment.

Intermittency frequencies are calculated by determining the number of times the intermittency function changes from 0 to 1 during a data record and dividing by the total collection time for the data record.

Once the intermittency function is available, conditionally sampled quantities are calculated for the turbulent region. The average methane concentration, standard deviation, skewness and kurtosis values for the turbulent fluid are calculated as described above for the entire data record.

All of the above discussion on concentration measurements has been in terms of volume (or mole) fractions. Often, the concentration fields of turbulent jets are given in terms of mass-fraction concentrations (for examples see Way & Libby 1971; Birch *et al.* 1978) in an attempt to allow the comparison of jets with varying density. The use of mass fractions automatically corrects for differences in jet behaviour due to momentum differences based on density. Birch *et al.* (1978) have given the following approximate equations for converting mole-fraction concentrations into mass-fraction terms:

$$\overline{Y}_{CH_4} = \frac{(\alpha_\rho + 1)\,\overline{X}_{CH_4}}{\alpha_\rho \overline{X}_{CH_4} + 1}, \tag{24}$$

$$Y'_{CH_4} = \frac{(\alpha_\rho + 1)\,X'_{CH_4}}{\alpha_\rho \overline{X}_{CH_4} + 1}, \tag{25}$$

where $\overline{Y}_{CH_4}$ is the average concentration of methane in mass-fraction terms, Y'_{CH_4} is the r.m.s. of the methane concentration fluctuations in mass-fraction terms, and $\alpha_\rho = \rho_{CH_4}/\rho_{air} - 1$ is the ratio of densities between pure methane and pure air minus one. Birch *et al.* have concluded that there are no measurable differences using mass or mole fractions for skewness, kurtosis, correlation functions, or power spectra.

5. Results

5.1. *Nature of detected Rayleigh scattering*

The average current output of the photomultiplier for scattering from air is measured to be $\sim 13\ \mu A$, of which $\sim 55\%$ is due to Rayleigh scattering from air, with the remainder being due primarily to scattered light from the enclosure. Using the gain value of the photomultiplier provided by the manufacturer, this corresponds to a photon detection rate of 3.4×10^7 photons/s or 1.9×10^7 photons/s for the Rayleigh scattering. This experimental value can be compared with the predicted value of 8.3×10^7 photons/s given in §2.3. Even though the two values differ by a factor of 4.3, the agreement is considered satisfactory since many of the parameters substituted in (14) are based on best-case estimates. Additionally, the gain of the photomultiplier may no longer be the same as originally determined by the manufacturer.

As indicated earlier, the relative uncertainty in a current (intensity) measurement from a photomultiplier is expected to be proportional to the square root of the cut-off frequency. Measurements of the standard deviation in detected intensity for a constant intensity source sufficient to generate a current of 15 μA were made for three cut-off frequencies. The relative errors are summarized in table 1. In each case the observed relative errors are $\sim 40\%$ higher than calculated using the quoted properties of the PMT. Much better agreement would be found if the photomultiplier gain is

Cut-off frequency (Hz)	Observed relative error	Calculated relative error
5700	0.028	0.019
2280	0.017	0.012
1140	0.011	0.009

TABLE 1. Observed and calculated relative errors as functions of cut-off frequency for the current from a photomultiplier illuminated by a constant-intensity light source

higher than the value used. Interestingly, a higher gain also leads to significant improvement in the agreement between the observed and calculated current for Rayleigh scattering from air.

Using the above results, it is possible to estimate the error in an individual methane concentration measurement when the actual concentration is $X_{CH_4} = 0.5$. X_{CH_4} is assumed constant for a time period which is greater than two times the inverse of the cut-off frequency. Assuming that the current detected for air is 13.0 μA and that for methane is 22.6 μA with 5.9 μA from background scattered light, the 50 % mixture of methane would be expected to give a signal of 17.8 μA with relative errors of 0.026, 0.016 and 0.010 for cut-off frequencies of 5700, 2280 and 1140 Hz respectively. Using these values, the uncertainties in the concentration measurement are calculated to be 4.8, 3.0 and 1.9 % of full scale. In actual practice, these values are expected to vary slightly as a function of operating conditions and methane concentration, but they represent a good estimate of the accuracy of a single methane concentration measurement with the experimental parameters of our experiment.

Figure 2 shows three 200 ms recordings of data at the same location in a turbulent flow of methane into air. These plots are uncorrected for photon statistics. The only parameter changed from one set of data to the next is the cut-off frequency of the amplifier which has values of (*a*) 5700, (*b*) 2850 and (*c*) 1140 Hz. Also included in figure 2 are the expected uncertainties in each concentration measurement based on photon statistics which are extrapolated from measurements of scattering from air. Fluctuations due to turbulent concentration changes are clearly visible in each plot, but as the cut-off frequency is decreased the uncertainty in each individual measurement is visibly reduced. Significantly, when (21) is used to calculate the r.m.s., skewness and kurtosis for the concentration fluctuations, the results for each of the three 32768 point data sets are in close agreement. This result indicates that the effects of fluctuations due to electronic shot noise can be deconvoluted from the time-averaged properties of the concentration distribution.

5.2. *Time-averaged properties of the methane-concentration field*

Our goal in this work is to demonstrate the effectiveness of Rayleigh scattering as a concentration probe in isothermal turbulent flows involving two different gases. As part of this study it is necessary to compare measured values of time-averaged concentration field properties with similar measurements made by other workers using different techniques and with the two past studies using Rayleigh scattering as a probe. For this reason, we have mapped out the centreline behaviour as a function of the axial downstream distance z from the nozzle, and the radial behaviour (in terms of the distance r from the centreline) of the jet for one downstream distance ($z = 111$ mm).

Figure 3 shows a plot of reciprocal methane concentration versus axial distance,

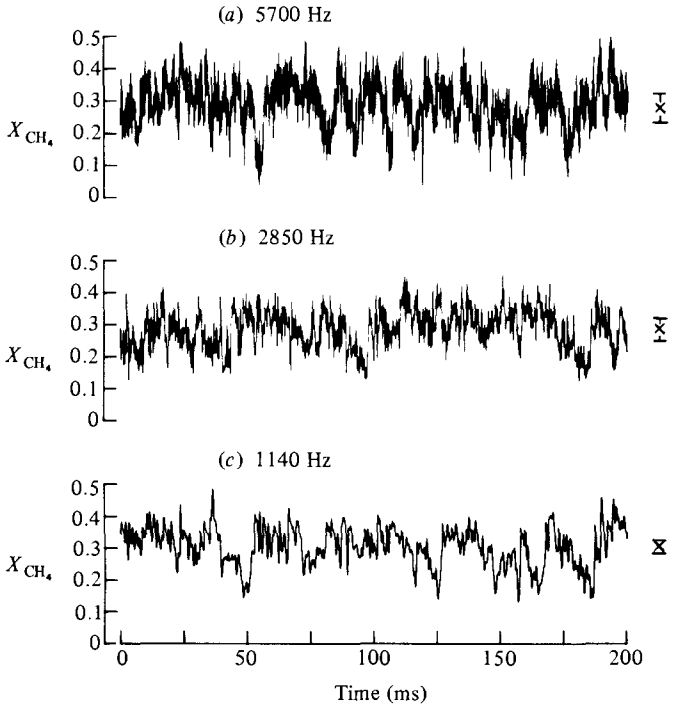

FIGURE 2. Appearance of data records for time-resolved light-scattering measurements as a function of cut-off frequency. The measurement volume is located on the jet axis at $z/r_0 = 35$. The vertical axis indicates methane concentrations, which are uncorrected for photon statistics. Average methane concentrations for the entire data sets are indicated by $\times$, and the expected r.m.s. fluctuations ($\pm 1\sigma$) due only to photon statistics are indicated by the bars.

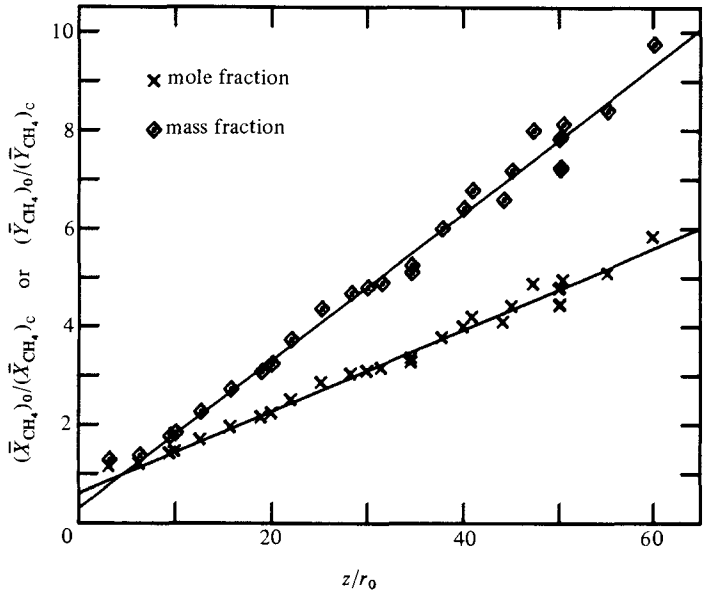

FIGURE 3. Values of $(\bar{X}_{CH_4})_0/(\bar{X}_{CH_4})_c$ and $(\bar{Y}_{CH_4})_0/(\bar{Y}_{CH_4})_c$ are plotted as functions of z/r_0. Solid lines are the results of linear least-squares fits for measurements taken at $z/r_0 \geqslant 20$.

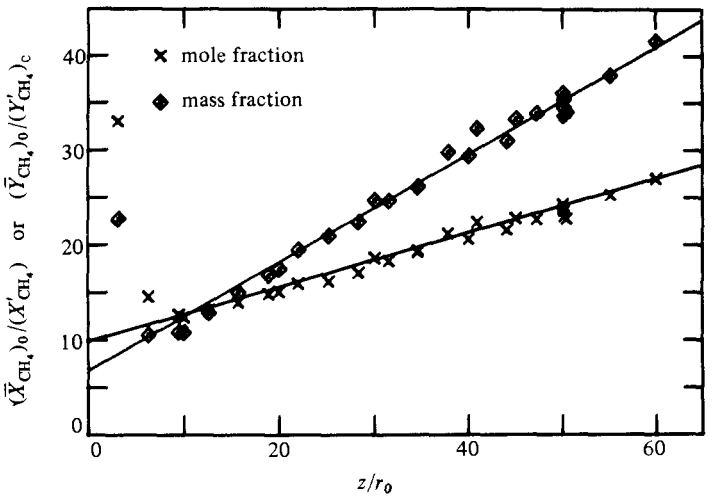

FIGURE 4. Values of $(\bar{X}_{CH_4})_0/(X'_{CH_4})_c$ and $(\bar{Y}_{CH_4})_0/(Y'_{CH_4})_c$ are plotted as functions of z/r_0. Solid lines are the results of linear least-squares fits for measurements taken at $z/r_0 \geqslant 20$.

which has been non-dimensionalized by dividing z by the nozzle radius r_0. Note that the concentration of methane is given in both mole fraction $\bar{X}_{CH_4}$ and mass-fraction $\bar{Y}_{CH_4}$ terms. The straight lines drawn through the data points are the results of linear least-squares curve fits of the data for $z/r_0 > 20$. To facilitate later comparisons, the dependence of mole fraction concentration on downstream distance is expressed in the form

$$\frac{(\bar{X}_{CH_4})_0}{(\bar{X}_{CH_4})_c} = \frac{C_1^X(z-z_0^{1X})}{r_0}, \tag{26}$$

where $(\bar{X}_{CH_4})_0$ is the concentration of methane at the nozzle exit ($(\bar{X}_{CH_4})_0 = 1$), the subscript c indicates measurements on the jet centreline, C_1^X is a constant, and z_0^{1X} is the virtual origin in mole-fraction terms. A similar equation is used for the mass-fraction results:

$$\frac{(\bar{Y}_{CH_4})_0}{(\bar{Y}_{CH_4})_c} = \frac{C_1^Y(z-z_0^{1Y})}{r_\epsilon}, \tag{27}$$

where $r_\epsilon = r_0(\rho_{CH_4}/\rho_{air})^{\frac{1}{2}}$ is an effective radius used by Birch *et al.* (1978) in an effort to account for density differences between the methane and air. This concept was originally introduced by Thring & Newby (1953), and does seem to provide a good correction for density effects due to differences in temperature (Wilson & Danckwerts 1964). C_1^X is found to equal 0.083 with $z_0^{1X} = -7.5r_0$, the fit of (27) gives $C_1^Y = 0.112$ with $z_0^{1Y} = -2.0r_0$.

Values of the r.m.s. concentration fluctuations as a function of axial distance are shown in figure 4 for both mole- and mass-fraction representations. These data also seem to fall on straight lines. The two sets of data are fit to equations of the same form as (26) and (27), namely

$$\frac{(\bar{X}_{CH_4})_0}{(X'_{CH_4})_c} = \frac{C_2^X(z-z_0^{2X})}{r_0} \tag{28}$$

and

$$\frac{(\bar{Y}_{CH_4})_0}{(Y'_{CH_4})_c} = \frac{C_2^Y(z-z_0^{2Y})}{r_0}. \tag{29}$$

The data shown in figure 4 give $C_2^X = 0.29$ with $z_0^{2X} = -35r_0$ and $C_2^Y = 0.57$ with $z_0^{2Y} = -12r_0$.

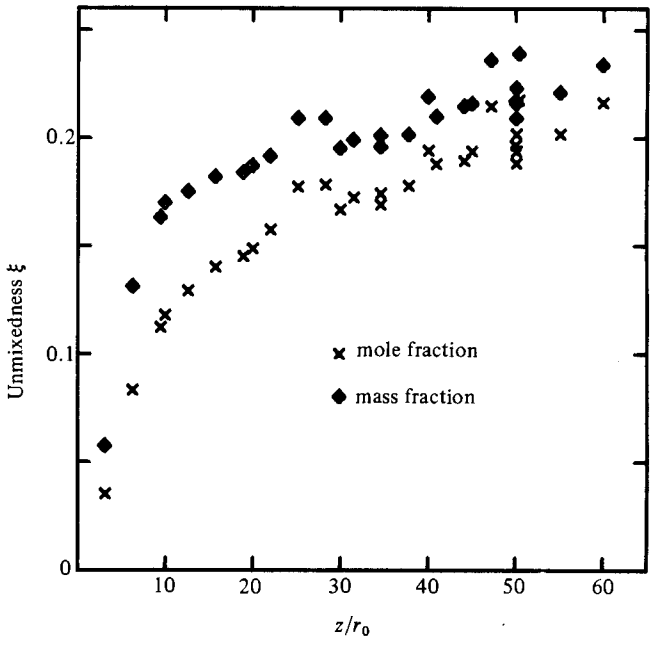

FIGURE 5. Unmixedness of methane concentration on the jet centreline in mole- and mass-fraction terms is plotted as a function of z/r_0.

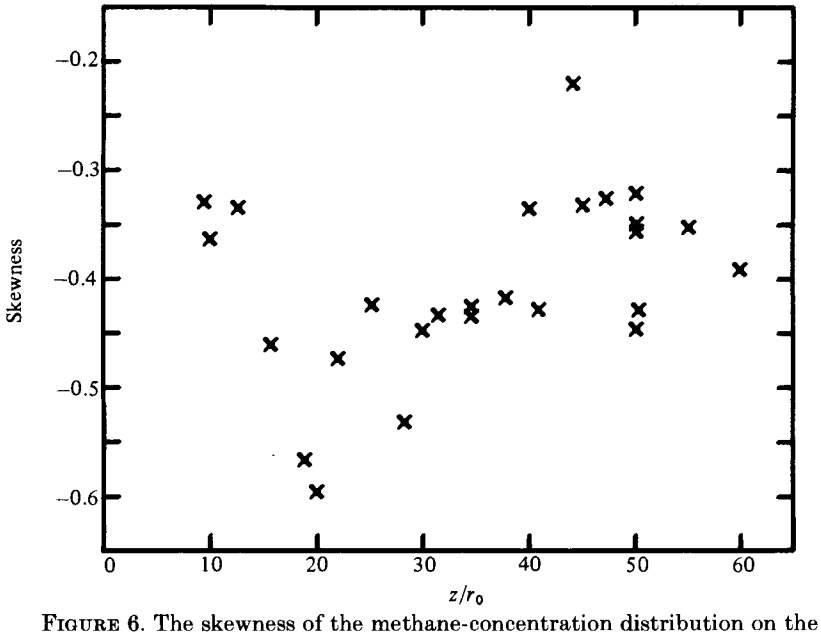

FIGURE 6. The skewness of the methane-concentration distribution on the jet centreline is plotted as a function of z/r_0.

Often the behaviour of r.m.s. turbulent fluctuations is described in terms of fluctuation intensities. Concentration-fluctuation intensity is defined as the local r.m.s. of the concentration fluctuation divided by the local average concentration, $X'_{CH_4}/\overline{X}_{CH_4}$ or $Y'_{CH_4}/\overline{Y}_{CH_4}$. Concentration-fluctuation intensity is often called unmixedness. Figure 5 shows the concentration-fluctuation intensity along the jet centreline in both mole- and mass-fractions terms.

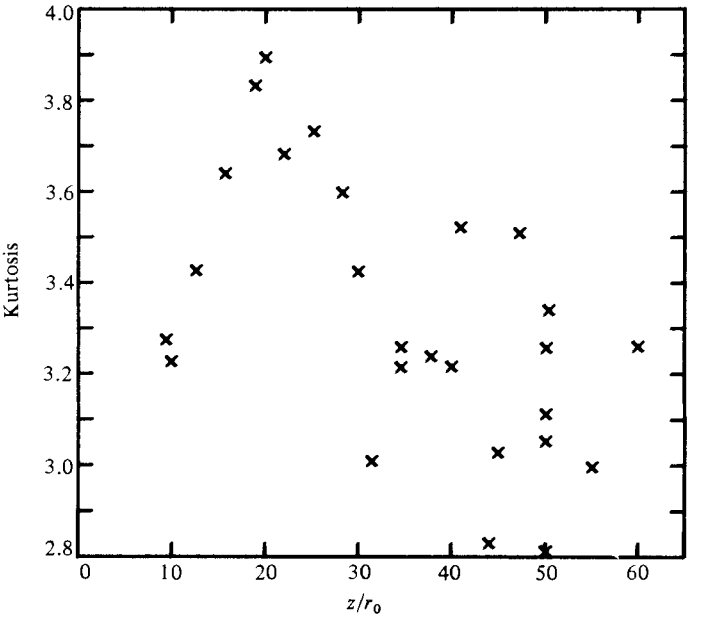

FIGURE 7. The kurtosis of the methane-concentration distribution on the jet centreline is plotted as a function of z/r_0.

The behaviours of the skewness and kurtosis factors as functions of z are shown in figures 6 and 7 respectively. Even though there are fairly large variations in the individual measurements, several distinct trends are evident in these results. The skewness is less than zero over the entire range of z-values investigated. The skewness seems to reach a minimum at $z/r_0 \approx 20$ and then gradually increases. Similarly, kurtosis values reach a maximum of ~ 3.8 near $z/r_0 \approx 20$ and then fall to values in the 3.0–3.2 range as z increases. Note that both measures indicate a non-Gaussian distribution for the turbulent-concentration fluctuations along the centreline of an axisymmetric jet.

Autocorrelation functions and power spectra have been calculated for all measurements taken along the jet centreline. Figure 8 shows examples of these functions for three values of z. Note that the frequency spectra are plotted as a function of log (relative spectral density) versus log (frequency). All of these spectra are taken from data recorded with a 4.6 kHz cut-off frequency. This cut-off frequency appears as a sharp dip in spectral density at high frequency values. For small values of z ($z = 20$ mm, $z/r_0 = 6.3$) there is still some spectral density due to turbulent fluctuations at the point where the signal is attenuated by the filter. Clearly some spectral information will be lost. By the time the flow is monitored at moderate downstream distances ($z = 80$ mm, $z/r_0 = 25.2$) the high-frequency portion of the spectral density due to concentration fluctuations is greatly reduced. A plateau in the spectral density is evident before the sharp drop due to the filter. This plateau is the baseline due to the white noise associated with photon detection statistics. This trend is much more evident further downstream ($z = 159$ mm, $z/r_0 = 50.1$), where a wide plateau region is observed. The same power spectrum also shows a spike at 120 Hz which is an artifact due to a small frequency oscillation of the laser power. The spike is only observed at large values of z, where the total fluctuation intensity is becoming weaker.

Integral timescales have been calculated from the autocorrelation functions using (23). Figure 9 shows the behaviour of these timescales as a function of z/r_0. The

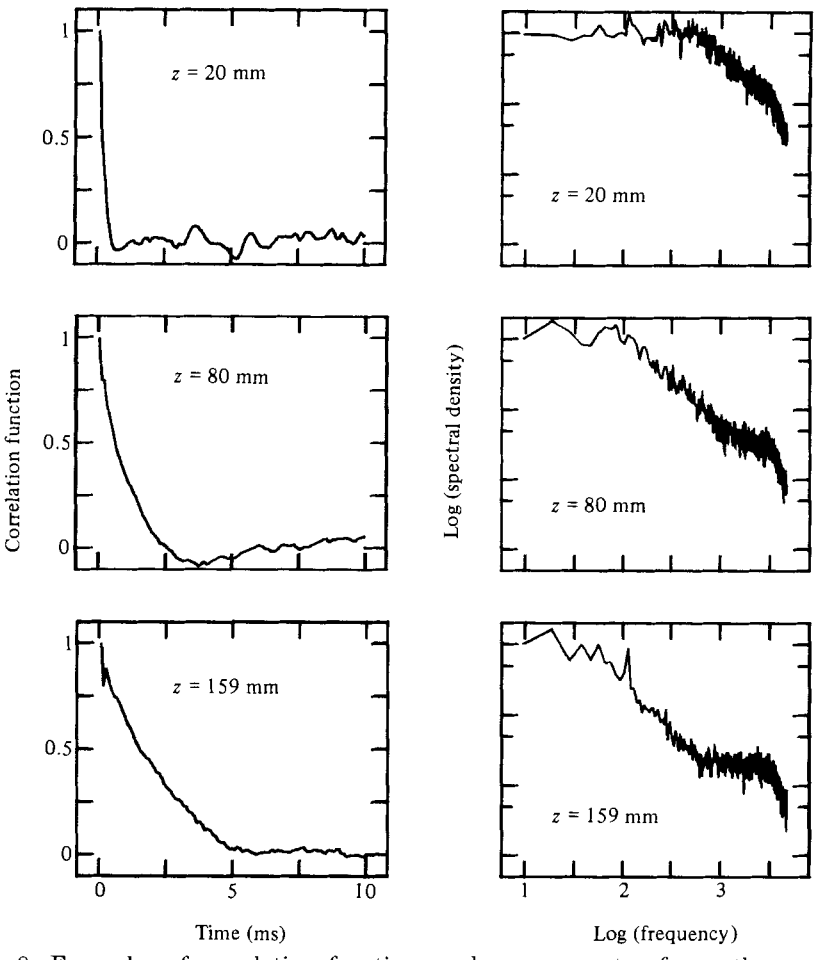

FIGURE 8. Examples of correlation functions and power spectra for methane-concentration fluctuations at three different axial downstream distances in a methane–air jet. The cut-off frequency of the amplifier is set to 4.6 kHz.

timescales clearly increase with downstream distance, but owing to the large variations between measurements it is impossible to give the form of the dependence. Birch *et al.* (1978) have shown that the timescales should increase as the square of the downstream distance. We attribute the large variations in measured integral timescales to digital noise which results when the autocorrelation is taken for discrete data recorded over a relatively short period of time. The digital noise appears as random fluctuations which result in errors for the exponential fit to the decay of the function. These fluctuations can be clearly seen in the autocorrelations shown in figure 8.

All of the measurements reported above are for $r = 0$. We have performed similar measurements for the radial behaviour of the concentration field at $z/r_0 = 35$. Figure 10 shows the average methane concentration as a function of r (normalized by $r_{\frac{1}{2}}$, the radial distance at which the concentration has decreased to one half of its centreline value). Both mole- and mass-fraction concentrations are included. The solid lines are Gaussian-type functions of the form

$$\frac{\overline{X}_{CH_4}}{(\overline{X}_{CH_4})_c} = \exp\left(-0.693\left(\frac{r}{r_{\frac{1}{2}}}\right)^2\right), \tag{30}$$

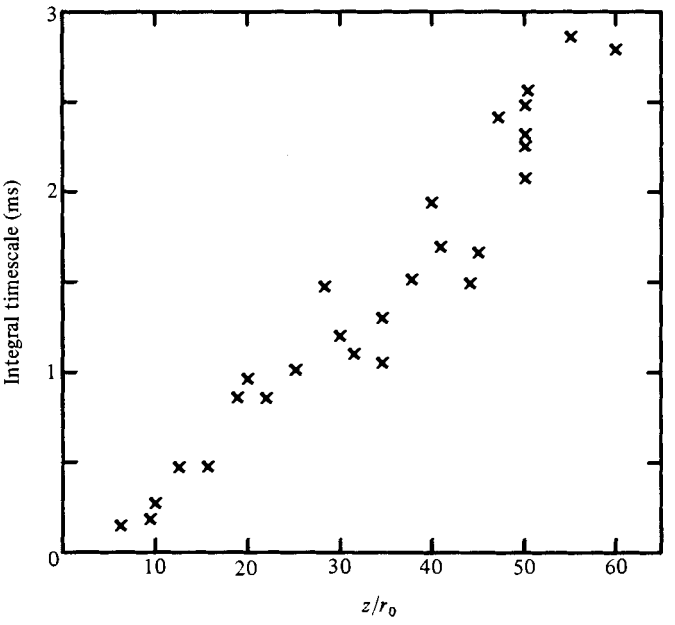

FIGURE 9. Integral time scales $\mathscr{T}$ on the jet centreline as a function of z/r_0.

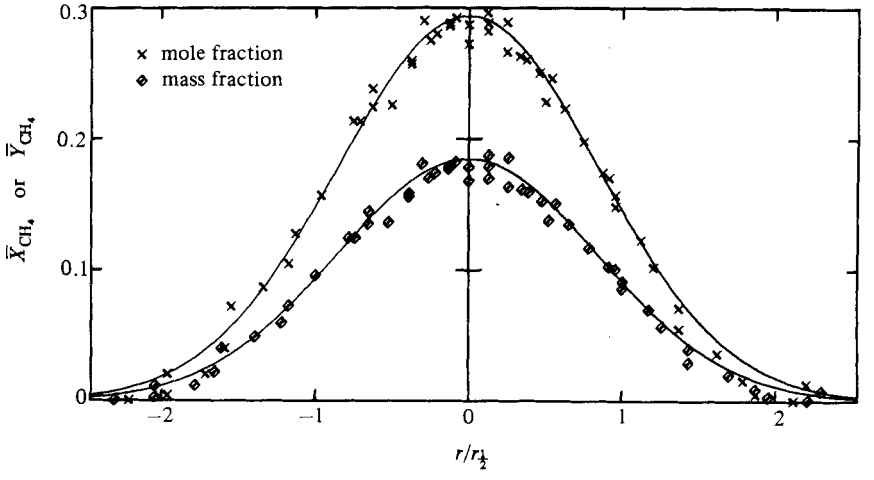

FIGURE 10. Behaviours of $\bar{X}_{CH_4}$ and $\bar{Y}_{CH_4}$ are shown as functions of non-dimensionalized radial distance $r/r_{\frac{1}{2}}$ for a downstream distance of $z/r_0 = 35$ in a methane–air jet. Solid lines are results for fits of (30).

where the only independent variables are the centreline concentration and $r_{\frac{1}{2}}$. Values of these two parameters are taken directly from the the data. These curves are in excellent agreement with both sets of data shown in the figure. Note that the values of $r_{\frac{1}{2}}$ used to fit the experimental values in figure 10 differ slightly. For mole-fraction concentrations $r_{\frac{1}{2}}/z = 0.108$, while the mass-fraction results give $r_{\frac{1}{2}}/z = 0.104$.

The r.m.s. concentration fluctuations normalized by the centreline value are shown in figure 11 in terms of mole and mass fractions. The solid line represents the results of Becker *et al.* (1967*b*) for an air–air axisymmetric jet and the dashed line gives the results of Birch *et al.* (1978) in terms of mass fraction for a methane–air jet. Note

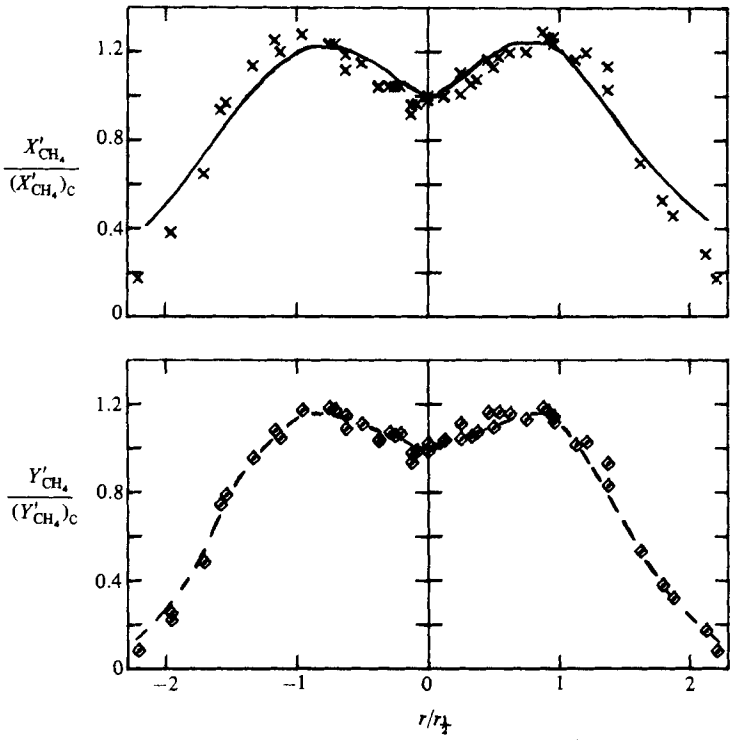

FIGURE 11. Experimental values of $X'_{CH_4}/(X'_{CH_4})_c$ and $Y'_{CH_4}/(Y'_{CH_4})_c$ are shown as functions of non-dimensionalized radial distance $r/r_{\frac{1}{2}}$ for a downstream distance of $z/r_0 = 35$ in a methane–air jet. The solid line represents results taken from the work of Becker *et al.* (1967*b*) for an air–air jet, and the dashed line gives the results of Birch *et al.* (1978) for a methane–air jet.

that the turbulent intensity initially increases as a function of r. $X'_{CH_4}/(X'_{CH_4})_c$ reaches a maximum of 1.31 at $r/r_{\frac{1}{2}} = 0.9$, while the r.m.s. concentration in terms of mass fraction only reaches a maximum of 1.18 at $r/r_{\frac{1}{2}} = 0.7$.

Figures 12 and 13 show plots of the skewness and flatness factors for the methane-concentration fluctuations as a function of $r/r_{\frac{1}{2}}$. Consistent with results in figure 6, the skewness on the jet centreline has a small negative value (~ -0.4), but as the measurement volume is moved outward in the radial direction the values of skewness continuously increase until near the edge of the jet they reach values greater than 5. As figure 13 reveals, the kurtosis value on the jet centreline is greater than the Gaussian value of 3. Initially, decreasing values of kurtosis are observed as the value of r is increased. This trend continues until the kurtosis has dropped to a value of ~ 2.5 at $r/r_{\frac{1}{2}} = 0.9$. After this minimum there is a rapid rise in kurtosis value, and near the outer wings of the jet values in excess of 30 are observed. These two figures also include the results for conditional measurements, which are described in §5.3.

Power spectra and autocorrelation functions have been calculated for the radial measurements. The behaviour of the integral timescales is shown in figure 14. Near the jet centreline the autocorrelation time is 1.5 ms, but, as the measurement volume is moved outward from the centreline of the jet, a monotonic increase occurs and the integral timescale increases to values greater than 10 ms in the outer region of the jet. It should be noted that the signal-to-noise ratio is greatly reduced for the autocorrelation function as the edge of the jet is approached. This is due to the fact

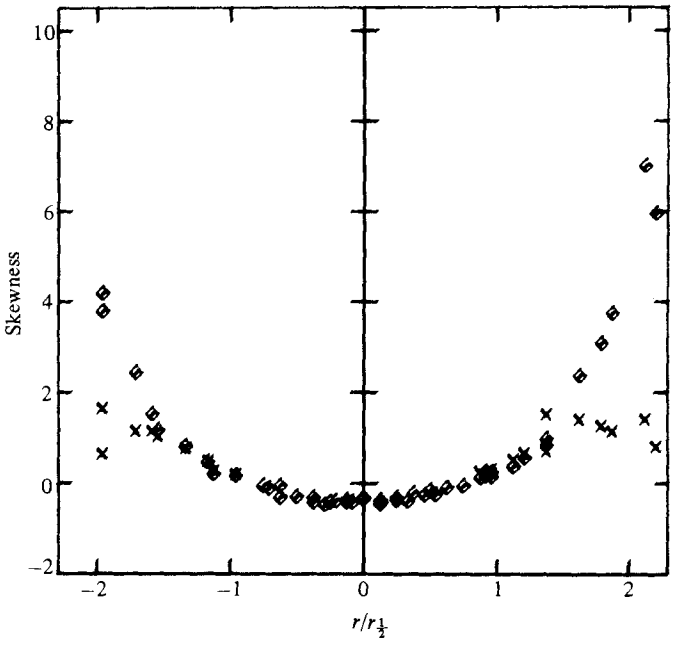

FIGURE 12. Skewness values as a function of non-dimensionalized radial distance $r/r_{\frac{1}{2}}$ are shown for the methane-concentration distribution at a downstream distance $z/r_0 = 35$ in a methane–air jet. Values have been calculated for entire data records (◇) and for conditionally sampled data, which are weighted by the corresponding intermittency functions (×).

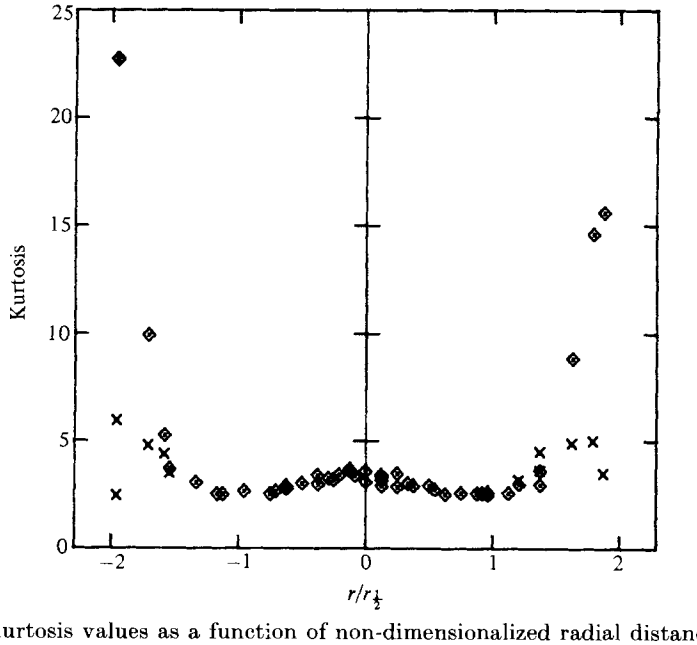

FIGURE 13. Kurtosis values as a function of non-dimensionalized radial distance $r/r_{\frac{1}{2}}$ are shown for the methane-concentration distribution at a downstream distance $z/r_0 = 35$ in a methane–air jet. Values have been calculated for entire data records (◇) and for conditionally sampled data, which are weighted by the corresponding intermittency functions (×).

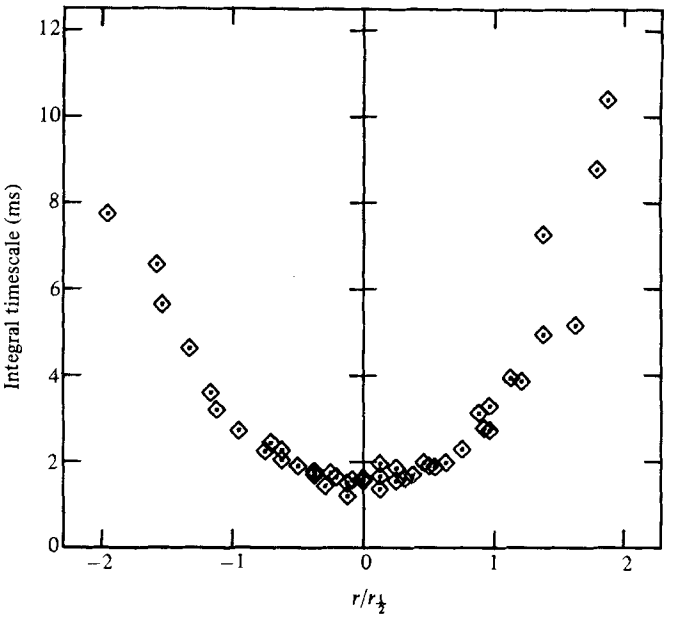

FIGURE 14. Integral timescales as a function of non-dimensionalized radial distance $r/r_{\frac{1}{2}}$ are shown for methane-concentration fluctuations at a downstream distance $z/r_0 = 35$ in a methane–air jet.

that only air is being monitored for a large fraction of the time. In these regions, fluctuations are only due to photon statistics, and since these are random they are uncorrelated and contribute a noisy zero baseline for the autocorrelation of the methane concentration fluctuations which occur during the fraction of time the fluid is turbulent.

5.3. *Conditional measurements in the methane-concentration field*

All of the calculations discussed thus far are for total data records. However, as discussed in §3, the fluid in the outer regions of the jet displays an effect known as intermittency, which results in two distinct types of fluid passing through the measurement volume element. The effect of intermittency is clearly seen in figure 15, where the methane concentration as a function of time is recorded for $z/r_0 = 35$ and $r/r_{\frac{1}{2}} = 1.25$. During part of the sweep the methane concentration is zero, while distinct 'bursts' of mixed fluid can be observed at other times. It should be noted that these bursts appear to result in sharp increases of methane concentration when they enter the measurement volume and that the methane concentration then seems to die away slowly until non-turbulent fluid is once again present. As discussed later, similar structures have been observed for the passive transport of heat in air–air jets.

The intermittency function calculated for the displayed portion of time-dependent methane concentration is also included in figure 15. Comparison of the observed methane concentration with the intermittency function shows that the algorithm described in §4.5 for intermittency determination gives a function which is in good visual agreement with the actual data. However, this figure also shows that very short bursts of turbulence (marked by arrows in the figure) are missed owing to the averaging process inherent in the intermittency determination. It is found that most of the turbulent bursts are of relatively long duration, and we therefore feel that the calculated intermittency functions are good representations of the actual behaviour of the flow.

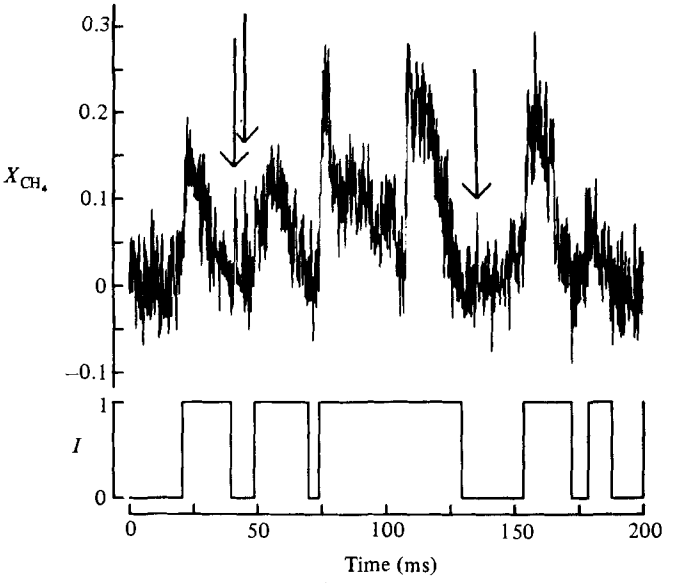

FIGURE 15. Example of methane-concentration behaviour in the intermittent region of a methane–air jet and the resulting intermittency function calculated for the data. Arrows indicate short 'bursts' of methane concentration which do not appear in the intermittency function owing to the averaging inherent in the calculation of this function.

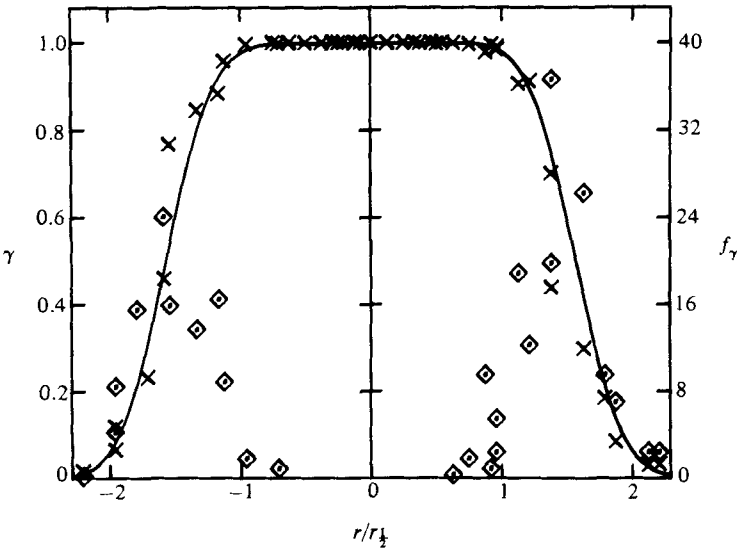

FIGURE 16. Intermittency factor γ and frequency f_γ as functions of non-dimensionalized radial distance $r/r_{\frac{1}{2}}$ for a downstream distance of $z/r_0 = 35$ in a methane–air jet. The solid line is a plot of (31) for $R = 1.6r_{\frac{1}{2}}$ and $\sigma_w = 0.28r_{\frac{1}{2}}$.

The intermittency factor γ has been calculated as a function of $r/r_{\frac{1}{2}}$, and the results are shown in figure 16 along with the corresponding intermittency frequency f_γ. The measurements are based on concentration in terms of mole fractions. These results are not expected to be very different for mass-fraction concentrations. It should be noted that values of f_γ are low and that they are subject to very large statistical error due to the few large-scale structures that passed through the observation volume

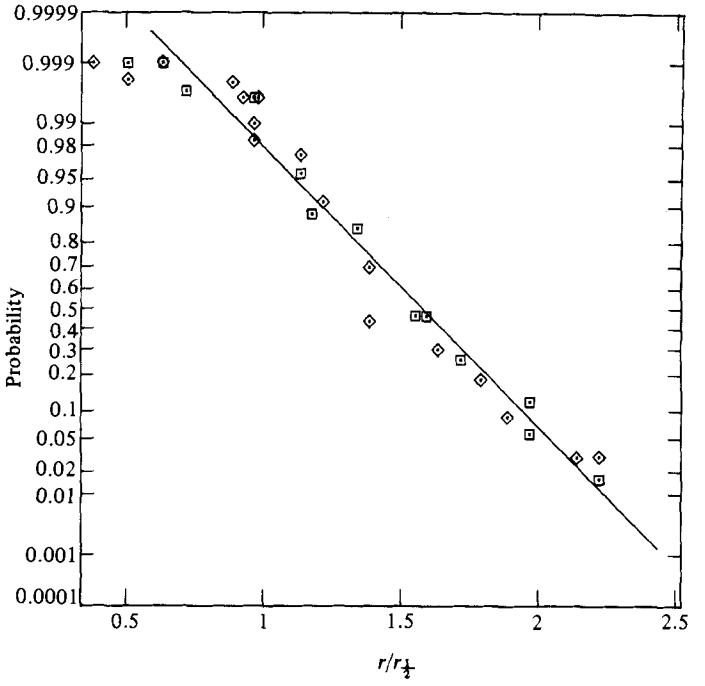

FIGURE 17. Values of the intermittency factor γ are plotted on a probability graph as a function of non-dimensionalized radial distance $r/r_{\frac{1}{2}}$. The solid line is a linear least-squares fit of all results except the five points closest to the jet centreline. The symbols refer to positive (◇) and negative (⊡) values of r.

during the 3.3 s data-collection time. This is especially true in the regions of very high or very low γ. The same argument indicates that measurements of γ will have large uncertainties in these regions also.

Several parameters can be defined that serve to characterize the behaviour of the intermittency function. For instance, the value of the normalized radial distance where $\gamma = 0.5$ is found to be $r/r_{\frac{1}{2}} = 1.6$. Within the accuracy of the experiment the maximum of f_γ also occurs at $r/r_{\frac{1}{2}} = 1.6$. Previous workers have found that when values of γ determined from the transport of passive markers are plotted versus $r/r_{\frac{1}{2}}$ on probability graphs, linear curves are found. Figure 17 shows such a plot for the values of γ that are included in figure 16. This plot is found to be linear for all values of γ except those where round-off errors in the measurements become significant. The linearity of this plot requires that the location of the outer boundary of the jet be purely random. An equation can be written to describe the behaviour of γ in terms of the average radial location of the jet edge ($\bar{R} = r$ where $\gamma = 0.5$) and the r.m.s. value for the movement of the jet edge relative to this value, $\sigma_w = (\overline{(R-\bar{R})^2})^{\frac{1}{2}}$ (Becker *et al.* 1967*b*). σ_w is sometimes called the 'wrinkle amplitude'. Using these definitions, the following equation can be written to describe the r-dependence of γ:

$$\gamma = 0.5 \operatorname{erfc}\left(\frac{r-\bar{R}}{\sqrt{2}\,\sigma_w}\right). \tag{31}$$

An analysis of the straight line in figure 17 gives $\bar{R} = 1.6 r_{\frac{1}{2}}$ and $\sigma_w = 0.28 r_{\frac{1}{2}}$. A plot of (31) is included in figure 16, and the agreement with experiment is very good.

Using intermittency functions such as that shown in figure 15, it is possible to calculate the average and higher central moments for concentration fluctuations in

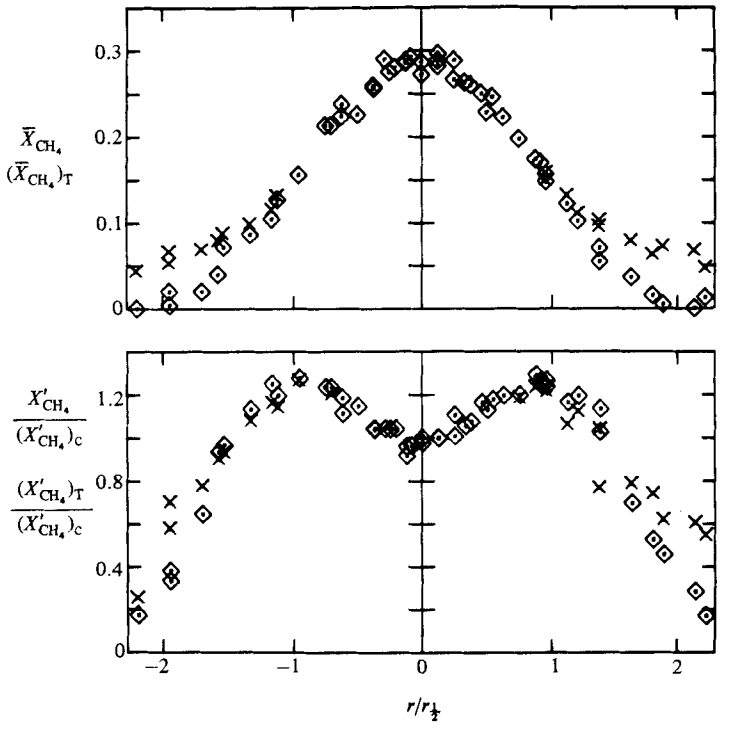

FIGURE 18. Plots of $\bar{X}_{CH_4}$ and $X'_{CH_4}/(X'_{CH_4})_c$ are given as functions of the non-dimensionalized radial distance $r/r_{\frac{1}{2}}$ at a downstream distance $z/r_0 = 35$ in a methane–air jet. The corresponding conditionally sampled values $(\bar{X}_{CH_4})_T$ and $(X'_{CH_4})_T/(X'_{CH_4})_c$ are indicated by the symbol $\times$.

the turbulent ($I(t) = 1$) regions. These calculations are performed in terms of mole-fraction concentrations. The general behaviour is expected to be the same if mass-fraction concentrations are used. Figure 18 shows plots of $\bar{X}_{CH_4}$ and $X'_{CH_4}/(X'_{CH_4})_c$ versus normalized radial distance along with the corresponding conditionally averaged quantities $(\bar{X}_{CH_4})_T$ and $(X'_{CH_4})_T/(X'_{CH_4})_c$. As would be predicted, the average methane concentration is higher in the turbulent fluid than for the non-conditioned average. The concentration in the turbulent bulges decreases much more slowly than the overall average concentration with radial distance. The conditionally sampled r.m.s. fluctuations as a function of normalized radius are decreased compared to the unconditioned results when γ is close to 1. However, as the value of γ decreases there is a crossover point at $r/r_{\frac{1}{2}} = 1.6$ for which $(X'_{CH_4})_T/(X'_{CH_4})_c$ is greater than 1.

The behaviours of conditionally sampled measurements of skewness and kurtosis are included in figures 12 and 13. The differences between conditionally sampled and overall measurements are striking at large values of r. This is not surprising, since in this region the fluid is 100% air for a relatively large fraction of the time and the lower end of the resulting methane-concentration distribution must be cut off at this point. Conditional measurements indicate that, while the skewness is still greater than zero and the kurtosis is greater than three in the turbulent regions, these parameters are constant or changing very slowly as a function of r.

6. Discussion

6.1. *Comparisons of measurements from this study with other work*

The primary goal of this study has been the demonstration of a new technique for performing space- and time-resolved measurements in turbulent flows. In the course of this work a large amount of data has been generated which can be analysed and compared with other work published in the literature. At the same time, we are confirming some past observations and reporting some new details of the behaviour of the concentration field of an axisymmetric jet. In most cases, comparisons are made with results for similar jets of air issuing into air where the concentration field is not mapped directly, but either heat (small temperature differences) or small particles are assumed to have been passive markers for concentration fluctuations. There is one detailed study (Birch *et al.* 1978) where Raman scattering has been used to map out the concentration-field behaviour for a free axisymmetric jet of methane. Raman scattering is not sensitive enough to allow actual time-resolved measurements such as the intermittency and conditionally averaged flow parameters reported here. However, by clever analysis of their data, the authors were able to obtain accurate averaged properties for the concentration field. Santoro *et al.* (1981) have used the promising new technique of optical tomography to measure the average concentration radial profile of a 10 % methane-in-air jet. The results reported in our work are in very good agreement with all of these past studies, despite the fact that many of the parameters which might be expected to affect turbulent behaviour (e.g. Reynolds number and initial flow conditions) vary in the different studies. Section 6.2 includes further discussion of this point.

6.1.1. *Concentration-moment analysis along jet centreline*

Equations (26) and (27) can be used to compare results of Rayleigh-scattering centreline-concentration measurements with those found in other studies. Table 2 compares values of C_1^X, z_0^{1X}, C_1^Y and z_0^{1Y} measured in this work with past measurements for air–air, methane–air and propane–air axisymmetric jets. The data for propane jets is calculated for only the three sets of axial data reported by Dyer (1979). C_1^X and z_0^{1X} for the data of Birch *et al.* (1978) are derived from results shown in figure 5 of their paper. There is no obvious relationship between the virtual origins of any of the measurements summarized in table 2, but it is interesting that all of the other studies report positive virtual origins while our work gives negative values. Bradshaw (1966) has argued that such differences are expected and depend on initial flow conditions. The most significant comparison of our results for centreline concentration behaviour should be with the work of Birch *et al.*, who also studied a methane–air jet. Comparison of C_1^Y values listed in table 2 shows that our value is $\sim 10\,\%$ smaller than the value found in the earlier work. However, these workers noted that the value of C_1^Y varies as the region of z/r_0 for which it is determined is changed. They speculated that this is due to a slow approach to similarity (where similarity is used here to mean the downstream behaviour of the centreline concentration can be specified simply by the reduced variable z/r_0). These workers found that a determination of C_1^Y over the same region of z/r_0 used in our work gave a value of 0.106, which is in good agreement with our results.

The results listed in table 2 are probably the most accurate available for the turbulent concentration fields of axisymmetric jets, but measured values are so scattered that it is impossible to distinguish whether plotting mole fraction or mass fraction gives the best agreement for jets of different-density gases. Becker *et al.*

Source	Jet	C_1^X	z_0^{1X}	C_1^Y	z_0^{1Y}	C_2^X	z_0^{2X}	C_2^Y	z_0^{2Y}	ζ_{mole}	ζ_{mass}
Present data	CH_4–air	0.083	$-7.5r_0$	0.112	$-2.0r_0$	0.29	$-35r_0$	0.57	$-12r_0$	0.29	0.27
Birch *et al.* (1978)	CH_4–air	0.090	$3.5r_0$	0.125	$11.6r_0$	—	—	0.58	$1.6r_0$	—	0.29
Dyer (1979)	propane–air	0.114	$5.1r_0$	0.090	$0.3r_0$	—	—	—	—	—	—
Becker *et al.* (1967*b*)	air–air	0.093	$4.8r_0$	0.093	$4.8r_0$	0.42	$-1.7r_0$	0.42	$-1.7r_0$	0.22	0.22

TABLE 2. Experimentally determined constants for (26)–(29) and asymptotic values for concentration-fluctuation intensity on the jet centreline in mole- and mass-fraction terms.

(1967*b*) reviewed experimental results in the literature for concentration and passive temperature fields of air–air jets and found that, even though C_1^X values seem to cluster near 0.1, the measurements show similar scatter to those given in table 2. Despite this apparent uncertainty in C_1^X values, it was claimed (Ebrahimi & Kleine 1977*a*) that a value of C_1^Y equal to 0.1 is a constant for isothermal and combusting jets. Clearly, more careful work is needed to determine whether or not a density effect is present in these studies and whether or not the use of the effective radius of Thring & Newby (1953) provides a suitable correction for changes in jet centreline behaviour as the density of the jet gas is changed owing to molecular composition.

Table 2 also includes the constants that describe the behaviour of r.m.s. concentration fluctuations on the jet centreline (see (28) and (29)). The agreement between the slope of the curve for our results in terms of mass-fraction concentration and that found by Birch *et al.* (1978) is excellent. These workers have concluded that r.m.s. concentration fluctuations approach similarity faster than the average concentration. This is consistent with our finding that C_2^Y values are in better agreement than C_1^Y for the two studies. This behaviour is the opposite of that found for the velocity flow field, where the average flow velocity approaches similarity faster than the r.m.s. fluctuations (Wygnanski & Fiedler 1969). Both of the experiments on methane jets give C_2^Y values that are in poor agreement with the results of Becker *et al.* (1967*b*) for an air–air jet. Note that no density correction is included in (29), and we are unaware of any method used to make such corrections for r.m.s. concentration fluctuations. However, the use of the effective-radius concept would improve the agreement. It is an interesting and as yet unexplained observation that the virtual origin shifts to more negative values for the r.m.s. fluctuations as compared to average centreline concentrations.

It should be noted that Lockwood & Moneib (1980) have reported measurements of temperature along the centreline of a heated axisymmetric jet. Even though the behaviours of the average and r.m.s. values are consistent with earlier results, the data were not analyzed in a manner similar to (26)–(29). For this reason, we have not compared our results with these recent measurements.

By dividing (26) by (28) and (27) by (29) it is possible to derive equations which give the concentration-fluctuation intensity ξ as a function of z for both mole- and mass-fraction measurements. For large values of z differences in the virtual origins become insignificant and $\xi_{\text{mole}} = C_2^X/C_1^X$ and $\xi_{\text{mass}} = C_2^Y/C_1^Y$. Table 2 includes the results of these calculations for air–air and methane–air jets. Note that the fluctuation intensity is relatively independent of whether or not mole- or mass-fraction concentrations are used. Table 2 indicates that the asymptotic value of ξ is dependent on density and that it is larger in the case of a methane–air jet as compared with an

air–air jet. Birch *et al.* (1978) reached the same conclusion and noted that the velocity-fluctuation intensity is also greater for the methane–air jet. This trend seems to hold for the limited data reported by Way & Libby (1971) for an axisymmetric jet of helium into air. Even though only two downstream axial locations were investigated, these authors reported a value $(Y'_{\mathrm{He}})_c/(\overline{Y}_{\mathrm{He}})_c$ of 0.37 at $z/r_0 = 40$. Lockwood & Moneib (1980) have argued that unmixedness should be independent of density ratio at high Reynolds number. They conclude that their value of $\xi_{\mathrm{air}} = 0.21$ is close to that expected for fully developed turbulent flow.

There is a paucity of measurements of skewness and kurtosis in the concentration fields of axisymmetric jets. The only results of which we are aware are due to Birch *et al.* (1978). These earlier results do not show the strong variations in skewness apparent in figure 6 for small z/r_0. Their results for $z/r_0 > 20$ have values of $S \sim -0.3$ and seem relatively constant over the $z/r_0 = 20$–60 range investigated in the current work. Our results seem to indicate an increase from $S \sim -0.6$ to $S \sim -0.35$ over the same range of z/r_0 values. Despite these minor differences, the agreement of these two sets of measurements must be considered good since each study indicates a negative skewness ($S = 0$ for a Gaussian) of approximately the same magnitude on the jet centreline. Similar agreement is found for the kurtosis measurements summarized in figure 7. Both studies find decreasing values of kurtosis which remain greater than 3 (the Gaussian value) throughout the entire range of z/r_0 values investigated. For an air–air flow marked with heat, Lockwood & Moneib (1980) also found a negative centreline skewness for all z-values investigated. However, while our results indicate an increasing skewness as z is increased, these authors find that S decreases. A more serious discrepancy occurs in the case of kurtosis measurements. For z/r_0 values greater than ~ 20, Lockwood & Moneib find K is nearly constant and equal to 2.9. Our results, as well as those of Birch *et al.*, indicate that $K > 3$ for all values of z. We cannot offer an explanation for these differences.

6.1.2. *Centreline power spectra and autocorrelation measurements*

At this time it is difficult to compare our power spectra, autocorrelation, and integral timescale measurements with other such measurements in the literature. As already noted, our measurements are susceptible to digital noise and fluctuations due to the short period of time for which data are collected. The general behaviour that we observe for the power spectra is consistent with the results in the literature where plots of log (spectral density) versus log (frequency) give a relatively flat region at low frequencies followed by a rapid fall-off at higher frequencies. We feel that our data collection and analysis procedures can be modified in order to obtain more accurate autocorrelation measurements.

6.1.3. *Moment analysis of radial concentration-fluctuation behaviour*

The radial profiles of average methane concentration in terms of mole and mass fractions are shown in figure 10. The experimental data are found to obey the Gaussian form of (30) quite well for values of $r/r_{\frac{1}{2}} < 1.5$. At larger values of $r/r_{\frac{1}{2}}$ the data seem to fall below the calculated curve, but definite statements are difficult due to uncertainties in the results arising from the short sampling times employed. Equations that are exactly equivalent to (30) have been used to model the radial concentration behaviour in air–air (Becker *et al.* 1967*b*), methane–air (Birch *et al.* 1978) and propane–air (Dyer 1979) jets. In addition, Shaughnessy & Morton (1977) and Santoro *et al.* (1981) have measured radial concentration profiles for air–air and 10% methane in air–air jets which are fitted well by (30). For the case of the air–air

Source	Jet	Concentration units	C_3	z_0
Present data	CH_4–air	mole	0.108†	0
			0.105†	$-9.1r_0$
		mass	0.104†	0
			0.103†	$-2.0r_0$
Birch *et al.* (1978)	CH_4–air	mass	0.097	0
Santoro *et al.* (1981)	10% CH_4–air	mole	0.097†	0
Dyer (1979)	propane–air	mole	0.086†	0
Becker *et al.* (1967*a*)	air–air	mole	0.106	$4.8r_0$
Wilson & Danckwerts (1964)	heated-air–air	mole	0.130	—

† From one downstream position

TABLE 3. Observed constants for spreading-rate behaviour (32) of axisymmetric jets

jet studied by Becker *et al.* (1967*b*), the authors claimed that at large values of $r/r_{\frac{1}{2}}$ ($\overline{X}_{\text{air}}/(\overline{X}_{\text{air}})_c < 0.08$) the experimental data fit was improved by using an equation that predicts a concentration fall-off with increasing r that is faster than Gaussian. This is consistent with our observations noted above. Clearly, the shape of the radial profiles for concentration behaviour are equivalent within experimental error for all axisymmetric jets investigated thus far. It should be noted that the results for a propane–air jet (Dyer 1979) are in terms of mole-fraction concentrations and those for the methane–air jet (Birch *et al.* 1978) are in mass-fraction terms. An analysis of the effect of transforming from mole fraction to mass fraction on the shape of the concentration radial profile indicates very little change in the overall shape of the profile, but the $r_{\frac{1}{2}}$ values shift to slightly smaller r-values for positively buoyant jets and to larger values for negatively buoyant jets. This can be seen in figure 10, where for the mole-fraction concentration $r_{\frac{1}{2}}$ is 12 mm and for the mass-fraction concentration case it is 11.5 mm.

Often the spreading rate of a jet is defined using $r_{\frac{1}{2}}$ values. For sufficient downstream distance the value of $r_{\frac{1}{2}}$ is found to be proportional to the distance from a virtual origin z_0. This relationship is written as

$$r_{\frac{1}{2}} = C_3(z - z_0), \tag{32}$$

where the values of C_3 and z_0 will be dependent on whether mole- or mass-fraction concentrations are used. Table 3 summarizes values of C_3 obtained for different jets using various experimental techniques. Dyer (1979) claimed that his value of C_3 indicates the presence of a slight density effect on the spreading rate of the jet. This conclusion may be correct, but such a definite statement is difficult to justify based on the limited data of table 3 which indicate very little difference between the air–air and methane–air jets. The results of Wilson & Danckwerts (1964) are for an air jet heated to 200 °C, and in this case heat may not be a passive marker. Their value of C_3 is much higher than the other values listed in table 3 for isothermal jets. Lockwood & Moneib (1980) have reported nearly identical results for their study of a heated (280 °C) air jet. The agreement of these two studies seems to indicate that heating the jet does change the spreading rate as compared to isothermal jets. Further work is required to clarify this point.

There does seem to be a density effect when concentration fluctuation r.m.s. values

Source	Jet	X'_{max}/X'_c	Y'_{max}/Y'_c	$r_{max}/r_{\frac{1}{2}}$
Present data	CH_4–air	1.31	—	0.92
	CH_4–air	—	1.18	0.70
Birch *et al.* (1978)	CH_4–air	—	1.20	0.7
Becker *et al.* (1967*b*)	air–air	1.15	1.15	0.8
Shaughnessy & Morton (1977)	air–air	1.14	1.14	0.9
Antonia *et al.* (1975)	air–air	1.19	1.19	1.0
Chevray & Tutu (1978)	air–air	1.21	1.21	0.95
Lockwood & Moneib (1980)	air–air	1.26	1.26	0.9
Dyer (1979)	propane–air	1.19	—	0.7
	propane–air	—	1.29†	0.8†

† Calculated from mole-fraction data given in paper

TABLE 4. Maximum normalized r.m.s. concentration-fluctuation values and radial locations for various axisymmetric jets

along the radial direction are considered. Figure 11 shows that the normalized radial r.m.s. values we observe are in close agreement with the methane–air results of Birch *et al.* (1978). One possible means of characterizing this type of measurement for different jets is to compare the values of the maximum ratio of X'_{max}/X'_c or Y'_{max}/Y'_c observed and the value of $r/r_{\frac{1}{2}}$ where it occurs. Table 4 lists the results from a number of different laboratories. Four sets of data are given for air–air jets in which passive markers were used as concentration probes. Becker *et al.* (1967*b*) and Shaughnessy & Morton (1977) both used light scattering from particles for their measurements. There is very good agreement between these two groups for both X'_{max}/X'_c and $r_{max}/r_{\frac{1}{2}}$. Antonia *et al.* (1975) and Chevray & Tutu (1978) have also studied air–air jets, but used heated air as a marker. These two groups of workers are also in good agreement, but the results obtained using the two different techniques are in relatively poor agreement, with the particle measurements giving smaller values for X'_{max}/X'_c and $r_{max}/r_{\frac{1}{2}}$. It may be that one of these techniques does not respond to turbulent fluctuations perfectly or that the markers are not totally passive. The results of Lockwood & Moneib (1980) for a heated air jet (255 °C) disagree with the other results for air–air jets. The source of this difference may be the strong heating of the air jet employed in the latter case. Despite these discrepancies, table 4 shows that the ratios X'_{max}/X'_c and Y'_{max}/Y'_c are greater for both methane and propane jets than for isothermal air–air jets. Owing to the discrepancy in the results for the air–air jets it is impossible to state whether or not there is a density effect on the value of $r_{max}/r_{\frac{1}{2}}$.

Our results for the skewness and kurtosis of concentration fluctuations as a function of $r/r_{\frac{1}{2}}$, shown in figures 12 and 13, are in excellent agreement with the results of Birch *et al.* (1978). Both the magnitudes of the parameters and their behaviour as a function of $r/r_{\frac{1}{2}}$ match closely. Our results are also in good agreement with those of Antonia *et al.* (1975) and Lockwood & Moneib (1980) for air–air jets. The rapid increases in both skewness and kurtosis values at the edge of the jet can be understood when it is noted that the intermittency factor rapidly falls off at approximately the same value of r where the large increases in S and K occur (compare figures 12 and 13 with 16). In this region of the flow field, periods of time during which the methane concentration is zero are averaged with those when the concentration is nonzero (this can be clearly seen in figure 15). Since the methane concentration cannot be negative, a sharp cut-off in the concentration distribution exists at the lower end and the

skewness and kurtosis values must increase dramatically as the fraction of time during which the fluid is pure air increases.

We have been unable to find detailed integral-timescale measurements as a function of r with which to compare the measurements shown in figure 14. However, Dyer (1979) did find that $\mathscr{T}$ increased from 140 μs to 315 μs on going from the centreline to $r_{\frac{1}{2}}$ in a propane–air jet. This observation is consistent with the results shown in figure 14.

6.1.4. *Description of fluctuation behaviour in the intermittent region of the concentration field*

No measurements of intermittency in the concentration field of an axisymmetric jet have been reported, but studies using passive markers have been performed. Becker *et al.* (1967*b*) studied the intermittency function for an air–air jet where the intermittency decision was based on light scattering from particles. These workers found that the radial location $\bar{R}$, where $\gamma = 0.5$, is equal to $\bar{R}/r_{\frac{1}{2}} = 1.78$. Using a similar technique, Shaughnessy & Morton (1977) found that $\bar{R}/r_{\frac{1}{2}}$ was 1.52 for an air–air jet with $Re = 56052$ and 1.43 with $Re = 31590$. Chevray & Tutu (1978) have performed detailed intermittency measurements in a heated air–air jet where the heat acted as a passive scalar. A value of $\bar{R}/r_{\frac{1}{2}} = 1.6$ can be inferred from their data. All of these values must be considered to be in good agreement with our measurement of $\bar{R}/r_{\frac{1}{2}} = 1.6$, since the value of $\bar{R}$ is highly dependent on the observation volume and cut-off constant used (see discussions in Antonia *et al.* 1975; Shaughnessy & Morton 1977).

It is difficult to compare our result for the wrinkle amplitude with the value measured by Becker *et al.* (1967*b*), since these workers found that the value of σ_w along the centreline is given by an equation with a different virtual origin than $r_{\frac{1}{2}}$. However, by assuming large values of z, a value of $\sigma_w/r_{\frac{1}{2}} = 0.29$ can be derived from their results. This value is in excellent agreement with the value of 0.28 determined in this study. In their study using heat as a marker, Antonia *et al.* (1975) found that σ_w was equal to $0.3r_{\frac{1}{2}}$, which is also in good agreement with our results.

As noted earlier, the concentration fluctuations in the intermittent region of the flow show a distinct ramp-like structure, which is clearly visible in figure 15. To our knowledge, this is the first observation of such structures in turbulent flows for an experiment monitoring concentration fluctuations directly. However, such structures have been found in studies using heat as a passive marker. As early as 1968 Gibson, Chen & Lin noted the presence of this behaviour in the wake of a heated sphere, where the sharp edge of the ramp occurred at the upstream end of the turbulent bulge. Similar structures in axisymmetric jets have been found to have the leading edge of the ramp facing downstream (Antonia *et al.* 1975). This observation is consistent with the time record of methane concentration fluctuations shown in figure 15, where the sharp edges of the ramp-like structures occur at the leading or downstream edge of the turbulent bulges.

The observation of these ramp-like structures in intermittent regions of turbulent flows has resulted in a wide range of studies which are beginning to yield detailed information concerning the behaviour of large-scale structures. Measurements of non-zero values of skewness in the derivative of temperature with respect to z, which can be obtained from $\partial T/\partial t$ by use of Taylor's hypothesis, have been associated with these ramp-like structures (for examples see Gibson, Friehe & McConnell 1977; Sreenivasan & Tavoularis 1980). Such observations are important, since one of the predictions of Kolmogorov's concept of local isotropy (Bradshaw 1971) is that the

skewness of $\partial T/\partial z$ will be zero. As might be expected, the sign of the derivative is found to depend on the type of flow configuration. The values are negative when the edge of the ramp faces downstream and positive when the face is upstream. Relations are being developed to predict the sign of the derivative based on measurements of average flow-field properties (Gibson *et al.* 1977; Sreenivasan & Tavoularis 1980).

Important clues to the nature of turbulent mixing have been derived from the work of Chevray & Tutu (1978) on heated axisymmetric jets. They used highly conditioned measurements to obtain average radial velocities near the beginning and end of the turbulent bulges. These workers have found that the average direction of fluid flow is away from the centre of the jet at the downstream edge of the bulges. This implies that highly concentrated gas from the centre of the jet is being 'shot out' into the surrounding fluid and thus explains the sharp edge of the ramp. At the upstream end of the ramp the average flow direction of the fluid is towards the centre of the jet. In this region the surrounding gas is being entrained into the jet and dilutes the jet fluid, leading to the fall-off in concentration as the bulge passes the observation volume. This proposed mechanism is described in a very lucid way by Gibson *et al.* (1977).

6.1.5. *Conditional measurements of methane concentration fluctuation behaviour*

Figure 18 shows that, as expected, the concentration of methane in the turbulent regions is considerably higher than the unconditioned concentration when the flow is intermittent. This same general behaviour has been observed in similar studies using passively marked air–air jets. Becker *et al.* (1967*b*) have given a numerical specification for $(\overline{X}_{\mathrm{air}})_{\mathrm{T}}/(\overline{X}_{\mathrm{air}})_{\mathrm{c}}$. For given $r/r_{\frac{1}{2}}$ values their turbulent concentrations are found to be significantly lower than those indicated in figure 18. For instance, at $r/r_{\frac{1}{2}} = 2$, this earlier work yielded a value of 0.15 for $(\overline{X}_{\mathrm{air}})_{\mathrm{T}}/(\overline{X}_{\mathrm{air}})_{\mathrm{c}}$, compared with a value of 0.29 taken from figure 18. This discrepancy is easily understood by noting that this earlier work found that the average location of the boundary of the jet occurs at $\overline{R}/r_{\frac{1}{2}} = 1.78$ as opposed to the value of 1.6 we have measured. Since the normalized wrinkle amplitude is nearly equal for the two jets, the value of γ at any normalized radius will be larger for the air–air jet. The radial profiles of concentration are nearly identical, which implies that at any given radial location the 'turbulent fluid' must contain a higher proportion of low-concentration jet fluid and the average concentration in the turbulent region will be lower. This conclusion is supported by the results of Chevray & Tutu (1978) for a temperature-marked jet. These workers found a normalized value of $\overline{R}/r_{\frac{1}{2}}$ which is nearly identical to that reported for the methane–air jet used here. The values of $(\overline{X}_{\mathrm{air}})_{\mathrm{T}}/(\overline{X}_{\mathrm{air}})_{\mathrm{c}}$ (where it must be remembered it is assumed that $\overline{X}_{\mathrm{air}}$ is proportional to a temperature difference) as a function of normalized radius are in very good agreement with the current measurements. For instance, at $r/r_{\frac{1}{2}} = 2$ these workers found a value of $(\overline{X}_{\mathrm{air}})_{\mathrm{T}}/(\overline{X}_{\mathrm{air}})_{\mathrm{c}} = 0.30$, which is very close to the value of 0.29 cited above. Based on these results, the current measurements of conditional concentrations must be considered in good agreement with the limited data available in the literature for passively marked air–air jets.

Data available for comparison with the conditional r.m.s. values shown in figure 18 are limited to the studies of Becker *et al.* (1967*b*) and Antonia *et al.* (1975). The general behaviour of the particle-marked air–air jet is similar to that shown in figure 18. Initially, as the mixing becomes intermittent the values of $(X'_{\mathrm{air}})_{\mathrm{T}}/(X'_{\mathrm{air}})_{\mathrm{c}}$ fall below the value of $X'_{\mathrm{air}}/(X'_{\mathrm{air}})_{\mathrm{c}}$. As the value of r is increased, the value of the conditioned r.m.s. again approaches that of the unconditioned r.m.s. and then becomes larger. The same general behaviour is found for the temperature-marked jet.

Source	Jet	ρ_{jet}/ρ_{air}	u_{air}/u_{jet}	Re
Present work	CH_4–air axisymmetric	0.55	0.033	4130
Birch *et al.* (1978)	CH_4–air axisymmetric	0.55	0	16000
Santoro *et al.* (1981)	10% CH_4–air axisymmetric	0.96	0	29000
Dyer (1979)	propane–air axisymmetric	1.52	0.033	9790
Becker *et al.* (1967*b*)	air–air axisymmetric	1.0	0	54000
Shaughnessy & Morton (1977)	air–air axisymmetric	1.0	0.024	56100
			0.042	31600
Antonia *et al.* (1975)	heated air–air axisymmetric	0.94	0.15	38000
			0.34	38000
			0.53	38000
Chevray & Tutu (1978)	heated air–air circular	0.94	0	34100
Lockwood & Moneib (1980)	heated air–air circular	0.54	0	50000

TABLE 5. Experimental parameters for different jets discussed in text

Interestingly, Antonia *et al.* find that the value of $(X'_{air})_T/(X'_{air})_c$ remains very nearly constant across the entire jet profile, in marked contrast to the results of figure 18 or the particle-marked air–air jet, where the intensity first rises and then falls for both the conditioned and conventional measurements. At this time we can offer no explanation for this difference, but we will note that Antonia *et al.* performed their study in a coflowing stream of air where the velocity ratio of the jet to surrounding gas was considerably lower than those used in this study or the free jet used by Becker *et al.* (1967*b*).

The only conditionally averaged skewness and kurtosis results of which we are aware for the radial distribution of concentration fluctuations is the work of Antonia *et al.* These workers find nearly identical behaviour for these two parameters as shown in figures 12 and 13. At r-values where both the skewness and kurtosis are rapidly increasing owing to intermittency, conditional measurements remain nearly constant. For both sets of measurements the conditioned value of skewness is positive and equal to approximately one, while the kurtosis value remains slightly higher than the Gaussian value of three.

6.2. *Validity of comparisons with other studies*

Up to this point, differences between our experimental flow conditions and those of studies with which our results are compared have not been considered in detail. Table 5 summarizes the conditions used in each of these studies for some of the parameters that might influence the measurements compared in §6.1. The values in the table are given in terms of the density ratio of the jet fluid to the surrounding air, the ratio of the air velocity ($u_{air} = 0$ is a free jet) to the jet velocity, and the Reynolds number based on the jet velocity and diameter.

From table 5 it is clear that the experiments used for comparison purposes with the results of this work have been performed under widely varying conditions. Despite these differences in flow conditions, very good agreement is found between our results and these earlier studies. In particular, the agreement between our results

and those of Birch *et al.* (1978) is very good, despite the fact that their jet was a free jet with a Reynolds number four times greater than that used for this work. The large differences in virtual origins recorded in table 2 also indicate that the initial conditions at the jet nozzles were very different for the two jets.

It is obvious that the use of an enclosure and a coflow of surrounding gas must change the concentration-field behaviour of the axisymmetric jet used in this study as compared with that of a free jet. As the jet slows down due to turbulent mixing with its surroundings, it will eventually decay to a velocity where it must respond to the coflow of air. The jet is also constantly expanding and will eventually fill the entire enclosure. However, in the downstream regions of the flow where we have made measurements, the effects of the coflowing surrounding gas and the enclosure do not seem strong enough to modify the concentration field in an experimentally verifiable way. The radial profile of the jet was studied at an axial position where the jet has a maximum radius of ~ 29 mm. (The outer edge of the jet spends 99.9 % of the time within this distance of the centreline, see figure 17.) Since the shortest distance from the jet centreline to the walls of the enclosure is 50.8 mm, it is not surprising that the presence of the walls does not modify the behaviour of the jet in a measurable way. The absence of an effect due to the coflowing surrounding gases on the averaged properties of a jet at comparable downstream distances to those employed here has been noted by Shaughnessy & Morton (1977). These workers found that their results for a coflowing air–air jet were in very good agreement with those of Becker *et al.* (1967*b*) for the corresponding free jet.

Ebrahimi & Kleine (1977*a*, *b*) have given a formula for the variation of C_1^Y with Re which can be written as

$$C_1^Y = (1.3(Re/10^4)+6)^{-1}. \tag{33}$$

Table 2 compares values of C_1^Y from four different measurements where the Reynolds number varies from 4130 to 56000. Using (33), the expected variation in C_1^Y is from 0.153 to 0.075. The results summarized in table 2 indicate a much smaller variation than this. Based on the results of our measurements and comparisons with others in the literature, we feel that a small Reynolds-number effect may be present for values of C_1^Y, but that this effect is hidden by variations in values of C_1^Y due to experimental conditions. Shaughnessy & Morton (1977) found very little effect on jet properties on going from $Re = 56050$ to $Re = 31590$. However, they did note a small, but reproducible, decrease in the half-widths of the average velocity, average concentration and the normalized value of $\overline{R}$ as Re was lowered. Antonia *et al.* (1975) have reported a similar behaviour, but the results may not be comparable with those of the other jets in table 5 due to the relatively high values of $u_{\text{air}}/u_{\text{jet}}$ used in this work. Effects of Re-differences on the other properties of the concentration field evaluated in our study have not been reported. All of the evidence cited above indicates that, while small effects of Re may be present in these measurements, these effects are not strong enough to invalidate the comparison of our results with the other studies discussed in §6.1.

The effects of density differences on the behaviour of the average concentration field and the r.m.s. have already been discussed in §6.1. The concept of an effective radius used in (27) is expected to compensate for density differences between jet fluids for comparisons of the axial behaviour of average mass-fraction concentration, but the variations in the measured results among different studies are so large that this has not been verified. A strong effect does appear in the behaviour of the r.m.s. concentration fluctuation. Careful studies should be performed to confirm and

characterize this density effect. The presence or absence of effects due to density differences on other properties of the flow field reported in this study cannot be verified due to insufficient data for comparison.

On the basis of the very good agreement of the measured properties of the concentration flow field from this study and those in other studies and the lack of experimental evidence indicating strong modifications of the field (with the possible exception of those due to the effects of jet density), we conclude that the measurements reported in §§5.2 and 5.3 are reasonable and give an accurate description of the concentration field of an axisymmetric jet.

6.3. *Applicability of Rayleigh light scattering as a scalar probe of turbulent flow fields*

In the past, many different measurement techniques have been used to make scalar measurements in turbulent flow fields. Some of these techniques have been discussed briefly in the expanded version of this report (Pitts & Kashiwagi 1983). All of these techniques have serious disadvantages, and no one experimental method has dominated the field. Concentration- and temperature-measurement methods have lagged far behind the corresponding velocity measurements, where hot-wire and laser anemometry have provided easily implemented and accurate velocity determinations.

This study has been designed to demonstrate the feasibility of using laser Rayleigh light scattering as a concentration probe in simple turbulent flow systems. The Rayleigh technique has previously been shown to be a powerful means of monitoring mass density, number density and temperature fields in carefully selected complex turbulent reaction systems (see references listed in §2.2). As suggested by the pioneering studies of Graham *et al.* (1974) and Dyer (1979), the work reported here has proved that Rayleigh light scattering is an excellent technique for performing quantitative time- (~ 200 μs) and space-resolved (~ 0.0003 mm^3) measurements in a two-gas turbulent flow system. A wide variety of turbulence properties have been investigated and the results have been shown to be in excellent agreement with those in the literature which were measured using independent techniques.

A necessary requirement for this technique to have a wide applicability is that it be useful for a large number of different gas mixtures. One of the reasons methane was chosen for this study is that it does not have an unusually strong Rayleigh-scattering cross-section relative to that of air. Most gas pairs have scattering cross-section ratios at least as large as that for methane–air, $\sigma_{CH_4}/\sigma_{air} = 2.34$, and many are considerably higher. For instance, the propane–air combination has a ratio of 13.5. Furthermore, most gases have scattering cross-sections which are the same order of magnitude (the very small cross-section for helium is an exception) as those for air and methane. This implies that the present experimental arrangement can be used to study a wide variety of two-component turbulent flows with temporal and spatial resolution comparable to those found for this study. Of course, some combinations of gases will not be suitable owing to their having cross-sections that are nearly identical. In order to determine whether or not a particular binary gas combination is suitable for study, an analysis similar to that developed in §2.3 can be performed. Our results indicate that this analysis will only provide an order-of-magnitude estimate of signal and noise levels, but it should be possible to relate the results of the calculation to those combinations of gases for which experiments have been previously done in order to obtain a more accurate estimate of expected signal and noise levels.

We conclude from the results of this study and the discussions above that Rayleigh scattering offers a useful and accurate method for quantitative scalar measurements in many simple flow systems. When its applications to global measurements in the combustion systems listed in §2.2 are included, it is clear that Rayleigh scattering can become a powerful tool for the analysis of scalar properties in turbulent flow fields.

6.4. *Rayleigh versus Raman scattering as a scalar probe*

Owing to the nature of the techniques, turbulence experimenters will often be required to choose between Rayleigh and Raman light scattering as non-intrusive probes for turbulent flow systems. The choice of the type of scattering measurements must be based on the nature of the flow and the properties which are to be determined. Peterson (1979) has indicated in his review that Raman scattering is widely accepted as a flow diagnostic while experiments using Rayleigh scattering are not widely used. We feel that this is unfortunate since there are many experimental conditions for which Rayleigh scattering should be superior owing to its large cross-sections relative to those for Raman scattering. For flow systems where either Rayleigh or Raman scattering can be used, such as the flow studied here, two-component heated flows, three-component isothermal flows and certain reacting flows, Rayleigh scattering should offer substantial advantages over Raman scattering. Consider the application discussed in this work. Birch *et al.* (1978) have performed essentially the same study using Raman techniques. These workers reported point measurements for the average, unmixedness, skewness, kurtosis, concentration probability functions and autocorrelation functions of the methane-concentration fluctuations in the jet. Our analysis indicates that, with the exception of the autocorrelation functions, the measurements described in §5.2 are in excellent agreement and of comparable quality with those of this earlier work. These workers have not reported the time required for making a single point measurement in the flow, but since vibrational Raman scattering is expected to be at least 1000 times weaker than Rayleigh scattering, the time required to obtain a measurement with equivalent signal to noise should be at least 1000 times longer. This implies a time approaching an hour to make a single measurement which was performed in three seconds using Rayleigh scattering. These considerations are not only important from an efficiency viewpoint. In cases where flows of expensive gases are being studied it is important to limit experimental time for cost effectiveness. The above discussion is with regard to CW Raman experiments. Similar constraints will apply to experiments using pulsed lasers.

When it is noted that Rayleigh scattering also allows time-resolved studies and that the experimental requirements for Rayleigh scattering are less stringent (i.e. no spectrometer is required for Rayleigh scattering), it is clear that Rayleigh scattering is the superior technique for applications where its use is suitable. Examples where Rayleigh scattering cannot be used are systems where a large number of different gases must be monitored or where intense scattering from particles (such as soot) or the apparatus does not allow the elastic scattering to be observed. In these cases, Raman scattering provides an excellent alternative.

6.5. *Final remarks*

This work has presented a detailed description and investigation of laser-induced Rayleigh scattering as a concentration probe in binary mixtures of isothermal turbulent flows. It has been demonstrated that the technique can be used to provide detailed properties concerning the concentration flow field. In addition, detailed information concerning the concentration field of an axisymmetric jet has been

provided which should aid in a more complete understanding of turbulent mixing. In the near future we hope to perform detailed density-effect studies on this flow configuration using Rayleigh scattering as the probe.

Even though we feel that Rayleigh scattering has been demonstrated to be a powerful technique, there are several improvements that would make it more universally useful for turbulence studies. Among these is the use of polarization effects to allow an additional scalar property to be measured. It should also be possible to extend the technique to two dimensions as has been done for particle nephelometry (Long, Chu & Chang 1981) and Raman scattering (Webber, Long & Chang 1979).

A major conclusion of this paper must be that none of the current techniques currently available for providing scalar measurements in turbulent flows provide the ideal experimental solution. However, it is also clear that, by judicious choice, an experimenter can find techniques for performing these measurements with an accuracy and detail which has only been possible recently. In this context, the Rayleigh light-scattering technique evaluated in this paper is an important addition to the turbulence researcher's arsenal of probes for scalar measurements.

We have been aided by helpful discussions with Dr Howard Baum of the Center for Fire Research and Drs James McMichael and Patrick Purtell from the Center for Chemical Engineering. Comments of Drs Alfons Weber and Ray Mountain concerning the manuscript have been most helpful.

REFERENCES

ANTONIA, R. A., PRABHU, A. & STEPHENSON, S. E. 1975 Conditionally sampled measurements in a heated turbulent jet. *J. Fluid Mech.* **72**, 455–480.

BECKER, H. A., HOTTEL, H. C. & WILLIAMS, G. C. 1965 Concentration intermittency in jets. In *Proc. 10th Symp. (Intl) on Combustion*, pp. 1253–1263. Combustion Institute.

BECKER, H. A., HOTTEL, H. C. & WILLIAMS, G. C. 1967*a* On the light scatter technique for the study of turbulence and mixing. *J. Fluid Mech.* **30**, 259–284.

BECKER, H. A., HOTTEL, H. C. & WILLIAMS, G. C. 1967*b* The nozzle-fluid concentration of the round, turbulent, free jet. *J. Fluid Mech.* **30**, 285–303.

BILL, R. G., NAMER, I., TALBOT, L., CHENG, R. K. & ROBBEN, F. 1981 Flame propagation in grid-induced turbulence. *Combust. Flame* **43**, 229–242.

BIRCH, A. D., BROWN, D. R., DODSON, M. G. & THOMAS, J. R. 1978 The turbulent concentration field of a methane jet. *J. Fluid Mech.* **88**, 431–449.

BRADSHAW, P. 1966 The effect of initial conditions on the development of a free shear layer. *J. Fluid Mech.* **26**, 225–236.

BRADSHAW, P. 1971 *An Introduction to Turbulence and Its Measurement.* Pergamon.

CHENG, R. K., BILL, R. G. & ROBBEN, F. 1981 Experimental study of combustion in a turbulent boundary layer. In *Proc. 18th Symp. (Intl) on Combustion*, pp. 1021–1029. Combustion Institute.

CHEVRAY, R. & TUTU, N. K. 1978 Intermittency and preferential transport of heat in a round jet. *J. Fluid Mech.* **88**, 133–160.

COOLEY, J. W. & TUKEY, J. W. 1965 An algorithm for the machine calculation of complex Fourier series. *Math. Comput.* **19**, 297–301.

DIBBLE, R. W. & HOLLENBACH, R. E. 1981 Laser thermometry in turbulent flames. In *Proc. 18th Symp. (Intl) on Combustion*, pp. 1489–1499. Combustion Institute.

DIBBLE, R. W., HOLLENBACH, R. E. & RAMBACH, G. D. 1980 Temperature measurement in turbulent flames via Rayleigh scattering. In *Laser Probes for Combustion Chemistry* (ed. D. R. Crosley), pp. 435–441. American Chemical Society.

DYER, T. M. 1979 Rayleigh scattering measurements of time-resolved concentration in a turbulent propane jet. *AIAA J.* **17**, 912–914.

EBRAHIMI, I. & KLEINE, R. 1977*a* The nozzle fluid concentration fluctuation field in round

turbulent free jets and jet diffusion flames. In *Proc. 16th Symp. (Intl) on Combustion*, pp. 1711–1723. Combustion Institute.

EBRAHIMI, I. & KLEINE, R. 1977*b* Konzentrationfelder in isothermen Luft-Freistrahlen. *Forsch. Ing.-Wes.* **43**, 25–30.

GIBSON, C. H., CHEN, C. C. & LIN, S. C. 1968 Measurements of turbulent velocity and temperature fluctuations in the wake of a sphere. *AIAA J.* **6**, 642–649.

GIBSON, C. H., FRIEHE, C. A. & MCCONNELL, S. O. 1977 Structure of sheared turbulent fields. *Phys. Fluids Suppl.* **20**, S156–S167.

GOLDSCHMIDT, V. W., MULEJ, D. & AJAGU, C. O. 1979 The velocity of the turbulent/non-turbulent interface in a plane jet. In *Proc. 5th Symp. on Turbulence* (ed. J. L. Zakin), pp. 427–434. Science Press.

GOULDIN, F. C. & DANDEKAR, K. V. 1982 Time resolved density measurements in premixed turbulent flames. *AIAA Paper* 82-0036.

GRAHAM, S. C., GRANT, A. J. & JONES, J. M. 1974 Transient molecular concentration measurements in turbulent flows using Rayleigh light scattering. *AIAA J.* **12**, 1140–1142.

KONRAD, J. H. 1976 An experimental investigation of mixing in two-dimensional shear flows with applications to diffusion-limited chemical reactions. *Project SQUID Tech. Rep.* CIT-8-PU.

LANDOLT-BÖRNSTEIN 1962 *Zahlenwerte und Funktionen aus Physik, Chemie, Astronomie, Geophysik, und Technik*, II. Band, 8. Teil, *Optische Konstanten*. Springer.

LOCKWOOD, F. C. & MONEIB, H. A. 1980 Fluctuating temperature measurements in a heated round free jet. *Combust. Sci. Tech.* **22**, 63–81.

LONG, M. B., CHU, B. T. & CHANG, R. K. 1981 Instantaneous two-dimensional gas concentration measurements by light scattering. *AIAA J.* **19**, 1151–1157.

MCCARTNEY, E. J. 1976 *Optics of the Atmosphere*. Wiley.

MÜLLER-DETHLEFS, K. & WEINBERG, F. J. 1979 Burning velocity measurements based on laser Rayleigh scattering. In *Proc. 17th Symp. (Intl) on Combustion*, pp. 985–992. Combustion Institute.

PETERSON, C. W. 1979 A survey of the utilitarian aspects of advanced flowfield diagnostic techniques. *AIAA J.* **17**, 1352–1360.

PIKE, E. R. 1969 Photon statistics. *Riv. Nuovo Cim.* **1** (Numero Speciale), 277–314.

PITTS, W. M. & KASHIWAGI, T. K. 1983 The application of laser-induced Rayleigh scattering to the study of turbulent mixing. *Natl Bur. Stand. Internal Rep.* NBSIR 83-2641.

PITZ, R. W., CATTOLICA, R., ROBBEN, F. & TALBOT, F. 1976 Temperature and density in a hydrogen–air flame from Rayleigh scattering. *Combust. Flame* **27**, 313–320.

ROBBEN, F. 1975 Comparison of density and temperature measurement using Raman scattering and Rayleigh scattering. In *Combustion Measurements in Jet Propulsion systems: Proc. Project SQUID Workshop, Purdue University, 22–23 May 1975* (ed. R. Goulard), pp. 179–195.

SANTORO, R. J., SEMERJIAN, H. G., EMMERMAN, P. J. & GOULARD, R. 1981 Optical tomography for flow field diagnostics. *Intl J. Heat Mass Transfer* **24**, 1139–1150.

SCHON, J. P. & CHARNAY, G. 1977 Conditional sampling. In *Masurement of Unsteady Fluid Dynamic Phenomena* (ed. B. E. Richards), pp. 291–325. Hemisphere.

SHAUGHNESSY, E. J. & MORTON, J. B. 1977 Laser light-scattering measurements of particle concentration in a turbulent jet. *J. Fluid Mech.* **80**, 129–148.

SREENIVASAN, K. R. & TAVOULARIS, S. 1980 On the skewness of the temperature derivative in turbulent flows. *J. Fluid Mech.* **101**, 783–795.

THRING, M. W. & NEWBY, M. P. 1953 Combustion length of enclosed turbulent jet flames. In *Proc. 4th Symp. (Intl) on Combustion*, pp. 789–796. Standing Committee on Combustion.

WAY, J. & LIBBY, P. A. 1971 Application of hot-wire anemometry and digital techniques to measurements in a turbulent helium jet. *AIAA J.* **9**, 1567–1573.

WEBBER, B. F., LONG, M. B. & CHANG, R. K. 1979 Two-dimensional average concentration measurements in a jet flow by Raman scattering. *Appl. Phys. Lett.* **35**, 119–121.

WILSON, R. A. M. & DANCKWERTS, P. V. 1964 Studies in turbulent mixing – II. A hot jet. *Chem. Engng Sci.* **19**, 885–895.

WYGNANSKI, I. & FIEDLER, H. 1969 Some measurements in the self-preserving jet. *J. Fluid Mech.* **38**, 577–612.